Electronic Supplementary Material (ESI) for ChemComm.

Supporting Information

Going Against the Flow: Os(II)-to-Ru(II) Energy Transfer in a Rod-like Polypyridyl Chromophore†

Baptiste Laramée-Milette and Garry S. Hanan*

† Département de Chimie, Université de Montréal, 5155 Ch. De la Rampe, Pavillon J.-A. Bombardier, Montréal, Québec, Canada, H3T 2B1.

Table of Contents

Experimental Procedures

Materials and instrumentation

All solvent and reagents were used as purchased without further purification before the reactions. OsO_4 and $RuCl_3.3H_2O$ was purchased from Pressure Chemical Corporation. All other reagents were purchased from Sigma-Aldrich. ACS grade solvents were purchased from VWR and Fisher.

Nuclear magnetic resonance (NMR) spectra were recorded in acetonitrile-d_3 and DMSO-d_6 at room temperature (r.t.) on a Bruker AV400 (400 MHz) spectrometer for ^{1}H NMR, at 100 MHz for ^{13}C NMR and 600 MHz for DOSY experiment, respectively. Chemical shifts (δ) are reported in part per million (ppm) relative to TMS, and are referenced to the residual solvent protons (δ = 1.94 ppm for acetonitrile-d_3 and 2.50 ppm for DMSO-d_6) and the carbon resonance (δ = 118.26 ppm for acetonitrile-d_3 and 39.52 ppm for DMSO-d_6) of the solvent.

All the photophysical measurements were carried out in deaerated acetonitrile at r.t. in sealed quartz cells. Absorption spectra were measured on a Cary 500i UV-Vis-NIR Spectrophotometer from Agilent Technologies. For luminescence spectra a Perkin Elmer LS 55 was used. The luminescence lifetime measurement was performed on an Edinburgh OB 900 single-photon counting spectrometer equipped with a Hamamatsu PLP2 laser diode as pulse (wavelength output: 408 nm; pulse width: 59 ps). Deconvolution of the luminescence spectra was performed by using PeakFit V. 4.12.00. In all the cases, the fit correlation (r^2) was ≥ 0.99, considering an interval of 95% confidence.

Accurate high-resolution mass spectrometry experiments (HR-MS) was performed on a micrOTOF-Q II mass spectrometer from Bruker Daltonics, in positive electrospray mode. Appropriate $[M\text{-}PF_6]^{n+}$ species were used for empirical formula determination, and exact masses were calculated using the Compass DataAnalysis V4.0 SP5 software package from Bruker Daltonics.

Electrochemical measurements were carried out in argon-purged purified dimethylformamide at room temperature with a BAS CV50W multipurpose potentiostat. The working electrode was a 3-mm diameter glassy carbon electrode from CH Instruments. The counter electrode was a Pt wire, and the pseudo-reference electrode was a silver wire. The reference was set using an internal 1 mM ferrocene/ferrocinium sample at 0.450 mV vs. SCE in dimethylformamide. The concentration of the compounds was about 1 mM. Tetrabutylammonium hexafluorophosphate (TBAP) was used as supporting electrolyte and its concentration was 0.10 M. Cyclic voltammograms of were obtained at scan rates of 50, 100, 200 and 500 mVs^{-1}, respectively. The criteria for reversibility were the separation between cathodic and anodic peaks, the close to unity ratio of the intensities of the

cathodic and anodic currents, and the constancy of the peak potential on changing scan rate. Square wave voltammetry was conducted with a sweep rate of 20 mVs^{-1} and a pulse amplitude, width and period of 50 mV, 50 ms and 200 ms, respectively.

Experimental uncertainties are as follows: absorption maxima, ±2 nm; molar absorption coefficient, 10%; redox potentials, ± 10 mV, emission maxima, ±2 nm; Diffusion-ordered spectroscopy, ±10 %. The microanalyses were performed at the Elemental Analysis Service of the Université de Montréal.

X-ray Structure Determination

X-Ray diffraction data collection for the metal complex **1** was carried out on a Bruker Venture Metaljet diffractometer equipped with an Oxford Cryosystem liquid N2 device, using Ga-Kα radiation (λ = 1.34139 Å). The cell parameters were determined (APEX2 software) from reflections taken from three sets of 100 frames, each at 1 s exposure. The structure was solved by direct methods using the program Olex2. The H-atoms were included in calculated positions and treated as riding atoms using Olex2 default parameters. The non-H atoms were refined anisotropically, using weighted full-matrix least-squares on F2. More details are provided in the Supporting Information. CCDC 1545195 contain the supplementary crystallographic data for this paper. These data can be obtained free of charge from The Cambridge Crystallographic Data Centre via www.ccdc.cam.ac.uk/data_request/cif.

Computational Details

Gaussian 09, Revision E.01 was used for all theoretical calculations discussed herein.[1] The molecular structure of the metal complexes was fully optimized with CPCM acetonitrile solvation model in absence of constraints at Density Functional Theory (DFT) level, using, when possible, the crystallographic data as the starting point for the optimization. In particular, the hybrid PBE0 functional,[2] casting 25% of HF exchange in the PBE functional was applied.[3] The double zeta valence basis set LANL2DZ was used for all atoms but the Re ones which were described by the Los Alamos pseudo potential and corresponding basis set.[4] No imaginary frequencies were obtained when frequency calculations on optimized geometries were performed. GaussView 5.0.9,[5] GaussSum 3.0[6] and Chemissian 4.30 software were used for data analysis, visualization and surface plots.[7]

Synthesis of the ligands and the metal complexes

The benzene-1,4-di-2,2':6',2"-terpyridin-4'-yl ligand (bistpy), the 1,10-phenanthroline-hpp (phen-hpp) ligand and the K_2OsCl_6 precursor were synthesized as previously described.[8] Unless otherwise stated, the solvents were removed under reduced pressure using a rotary evaporator.

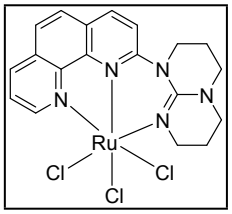

phen-hppRuCl$_3$

A 100 mL round-bottomed flask charged with ligand phen-hpp (315 mg, 1 mmol) and $RuCl_3.3H_2O$ (260 mg, 1 mmol) in EtOH (50 mL). The reaction mixture was left under reflux for 2 hours. After this time, the solution was cooled at -20°C. The resulting suspension was filtered over a 0.45 μm PTFE membrane, washed with EtOH (25 mL), acetone (25 mL) and

diethyl ether (50 mL). The burgundy precipitate was dried under vacuum for 1 hour and was used without further purification (273 mg, 52%).

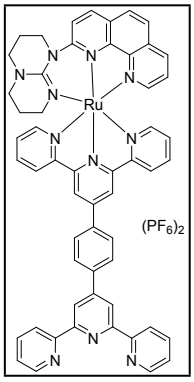

[bistpy(Phen-hppRu)][$(PF_6)_2$] (1)

A 20-mL microwave vial was charged with precursor **phen-hppRuCl$_3$** (50 mg, 0.10 mmol) and ligand bistpy (80 mg, 0.15 mmol) in ethylene glycol (20 mL) with 4-ethylmorpholine (16 drops). The reaction mixture was left under microwave irradiation (400W) for 15 minutes. The resulting purple solution was poured into an aqueous solution of KPF_6 (10 eq.) leading to instant precipitation of a deep purple precipitate. The heterogeneous solution was filtered over Celite®. The precipitate was washed with plenty of water and then dissolve in a minimum amount of acetonitrile. The organic fraction was then evaporated to dryness. The residue was purified on silica column, using a MeCN:H_2O:KNO_3 sat. mixture in a 20:1:1 ratio containing 1% of triethylamine. The brown band was recovered and the volume reduced under vacuum to ± 10 mL. Metathesis with aqueous KPF_6 solution was performed. The precipitate was extracted with methylene chloride (4 x 25 mL). The organic fraction was dried over anhydrous $MgSO_4$ and filtered over paper. The resulting solution was evaporated to dryness and the residue dissolved in a minimum amount of acetonitrile (5 mL). Addition of diethyl ether led to the precipitation of the mononuclear species **2**. The brown precipitate was recovered by filtration over a 0.45 µm PTFE membrane (24 mg, 22 %).

^{1}H NMR (400 MHz, CD_3CN): δ (ppm) = 8.97 (s, 2H), 8.93 (s, 2H), 8.86 (d, *J* = 9 Hz, 1H), 8.79-8.76 (m, 4H), 8.60 (d, *J* = 8 Hz, 2H), 8.39 (d, *J* = 8 Hz, 2H), 8.32-8.28 (m, 4H), 8.10 (d, *J* = 9 Hz, 1H), 8.06-8.01 (m, 3H), 7.93 (t, *J* = 8 Hz, 2H), 7.53-7.47 (m, 5H), 7.37 (dd, *J* = 7 Hz, 1H), 7.20 (t, *J* = 7 Hz, 2H), 4.09 (t, *J* = 6 Hz, 2H), 3.37 (t, *J* = 7 Hz, 2H), 3.04 (t, *J* = 6 Hz, 2H), 2.46 (m, 2H), 2.32 (m, 2H), 1.31 (m, 2H).

^{13}C NMR (100 MHz, CD_3CN): δ (ppm) = 159.3, 158.3, 154.3, 153.7, 146.1, 138.3, 137.7, 136.4, 131.3, 128.34, 128.26, 127.9, 127.0, 125.5, 124.9, 122.2, 49.7, 49.4, 49.2, 47.9, 47.7, 24.1, 23.1, 9.2.

HR-MS (ESI): m/z $[M\text{-}PF_6]^+$ calcd for $C_{55}H_{43}N_{11}RuPF_6$: 1104.23973; found: 1104.23885; difference: 0.80 ppm.

Calc. for $C_{55}H_{43}N_{11}RuP_2F_{12}.CH_2Cl_2$: C, 50.42; H, 3.40; N, 11.55. Found: C, 50.24; H, 3.67; N, 11.92%.

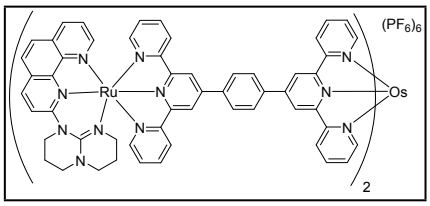

[$(bistpy(Phen\text{-}hppRu))_2Os$][$(PF_6)_6$] (2)

A 20-mL microwave vial was charged with precursor **1** (50 mg, 0.04 mmol) and K_2OsCl_6 (9.6 mg, 0.02 mmol) in ethylene glycol (20 mL) with 4-ethylmorpholine (16 drops). The reaction mixture was left under microwave irradiation (400W) for 15 minutes. The resulting deep purplish solution was poured into an aqueous solution of KPF_6 (10 eq.) leading to instant precipitation of a deep colored precipitate. The heterogeneous solution was filtered over Celite®. The precipitate was washed with plenty of water and then dissolve in a minimum amount of acetonitrile. The organic fraction was then evaporated to dryness. The residue was purified on silica column, using a MeCN:H_2O:KNO_3 sat. mixture in a 20:1:1 ratio containing 1% of triethylamine. The purplish band was recovered and the volume reduced under vacuum to ± 10 mL. Metathesis with aqueous KPF_6 solution was performed. The precipitate was extracted with methylene chloride (4 x 25 mL). The organic fraction was dried over anhydrous $MgSO_4$ and filtered over paper. The resulting solution was evaporated to dryness and the residue dissolved in a minimum amount of acetonitrile (5 mL). Addition of diethyl ether led to the precipitation of the trinuclear species **2**. The black precipitate was filtered over a PTFE membrane (25 mg, 42 %).

^{1}H NMR (400 MHz, CD_3CN): δ (ppm) = 9.22 (s, 4H), 9.05 (s, 4H), 8.89 (d, *J* = 9 Hz, 2H), 8.76 (d, *J* = 8 Hz, 4H), 8.67 (d, *J* = 8 Hz, 4H), 8.57 (d, *J* = 3 Hz, 8H), 8.33 (d, *J* = 9 Hz, 4H), 8.13 (d, *J* = 9 Hz, 2H), 8.07 (d, *J* = 9 Hz, 2H), 7.97 (t, *J* = 8 Hz, 4H), 7.89 (t, *J* = 8 Hz, 4H), 7.56 (d, *J* = 6 Hz, 4H), 7.52 (d, *J* = 5 Hz, 2H), 7.42-7.40 (m, 6H), 7.22 (dt, *J* = 7 Hz, 8H), 4.16-4.07 (m, 4H), 3.39 (t, *J* = 7 Hz, 4H), 3.07 (t, *J* = 6 Hz, 4H), 2.47 (m, 4H), 2.36 (t, *J* = 6 Hz, 4H), 1.34 (m, 4H).

^{13}C NMR (100 MHz, CD_3CN): δ (ppm) = 160.9, 159.3, 158.3, 156.1, 154.3, 153.6, 153.5, 152.8, 152.2, 147.4, 147.1, 146.1, 138.9, 138.5, 138.3, 136.3, 131.2, 130.1, 129.5, 128.7, 128.4, 127.9, 127.0, 125.8, 125.4, 124.9, 122.3, 121.3, 49.7, 49.4, 49.2, 48.0, 47.6, 24.1, 23.0, 9.1.

HR-MS (ESI): m/z $[M-4PF_6]^{+4}$ calcd for $C_{110}H_{86}N_{22}Ru_2OsP_2F_{12}$: 599.60983; found: 599.60976; difference: 0.12 ppm; $[M-2PF_6]^{+2}$ calcd for $C_{110}H_{86}N_{22}Ru_2OsP_4F_{24}$: 1344.18439; found: 1344.18690; difference: 1.87 ppm; $[M-PF_6]^{+}$ calcd for $C_{110}H_{86}N_{22}Ru_2OsP_5F_6$: 2833.33350; found: 2833.33132; difference: 0.77 ppm

Calc. for $C_{110}H_{86}N_{22}Ru_2OsP_6F_{36}.CH_2Cl_2$: C, 43.53; H, 2.90; N, 10.06. Found: C, 43.72; H, 3.29; N, 9.98%.

Results and Discussion

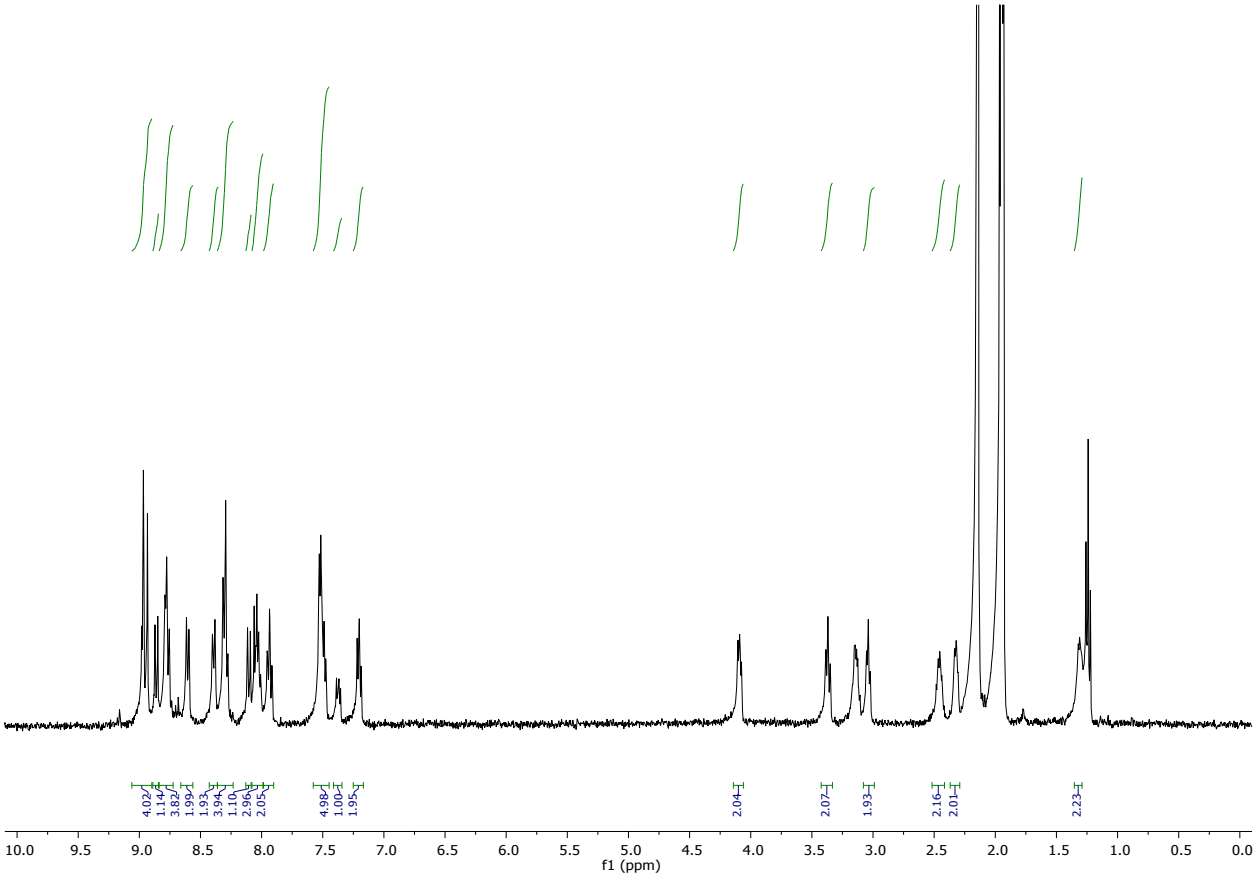

Figure S1. ^{1}H NMR spectra of **1** in acetonitrile-d_3.

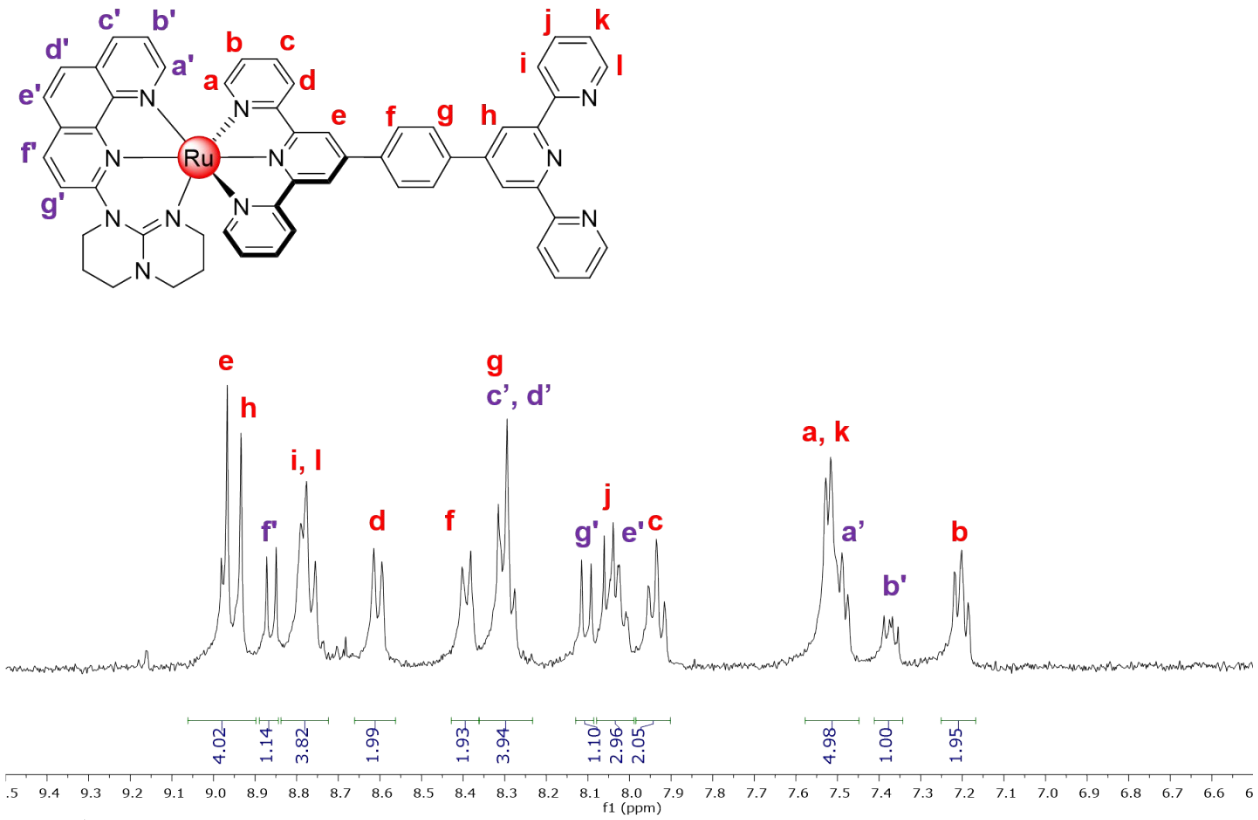

Figure S2. ^{1}H NMR spectra of the aromatic region of **1** in acetonitrile-d_3 with assignation of the signals.

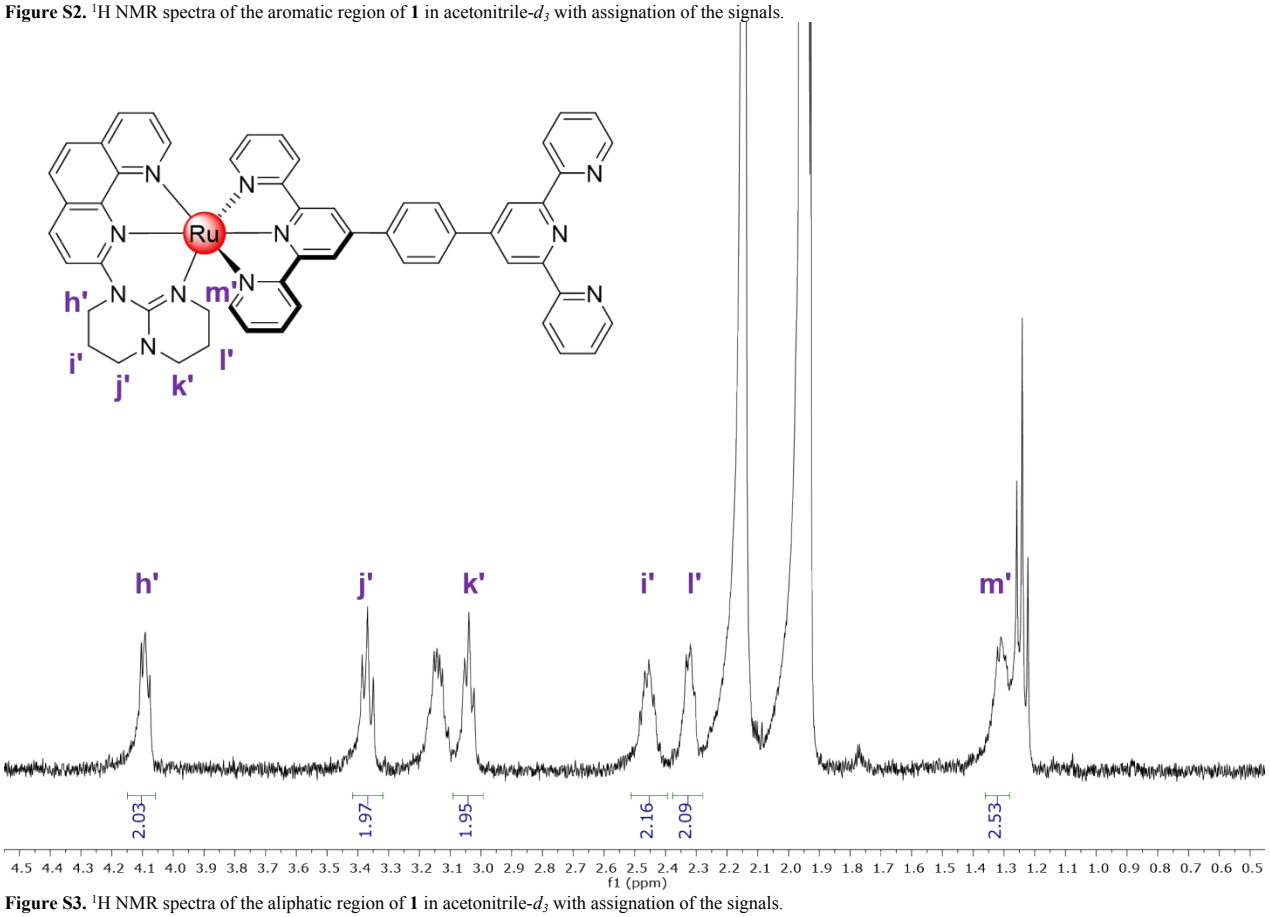

Figure S3. ^{1}H NMR spectra of the aliphatic region of **1** in acetonitrile-d_3 with assignation of the signals.

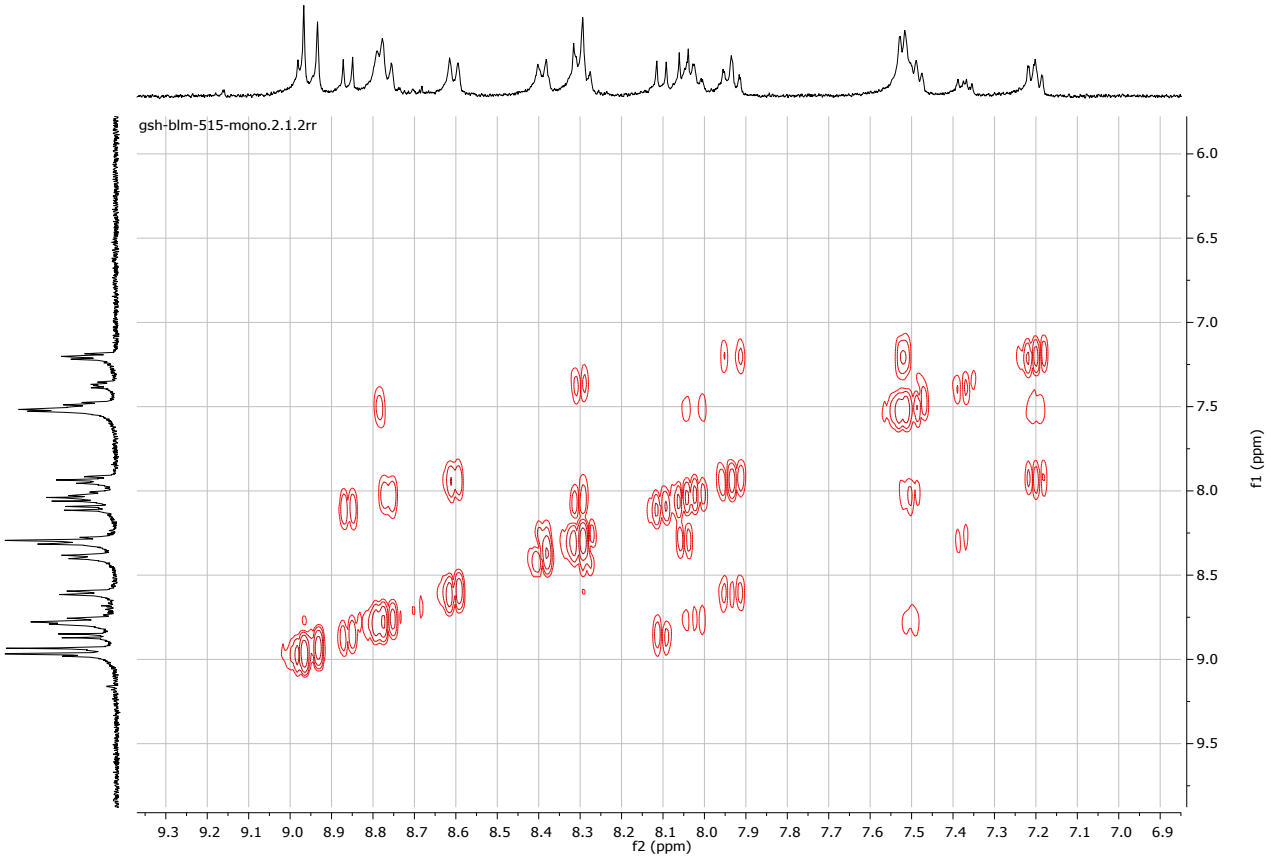

Figure S4. COSY spectra of the aromatic region of **1** in acetonitrile-d_3.

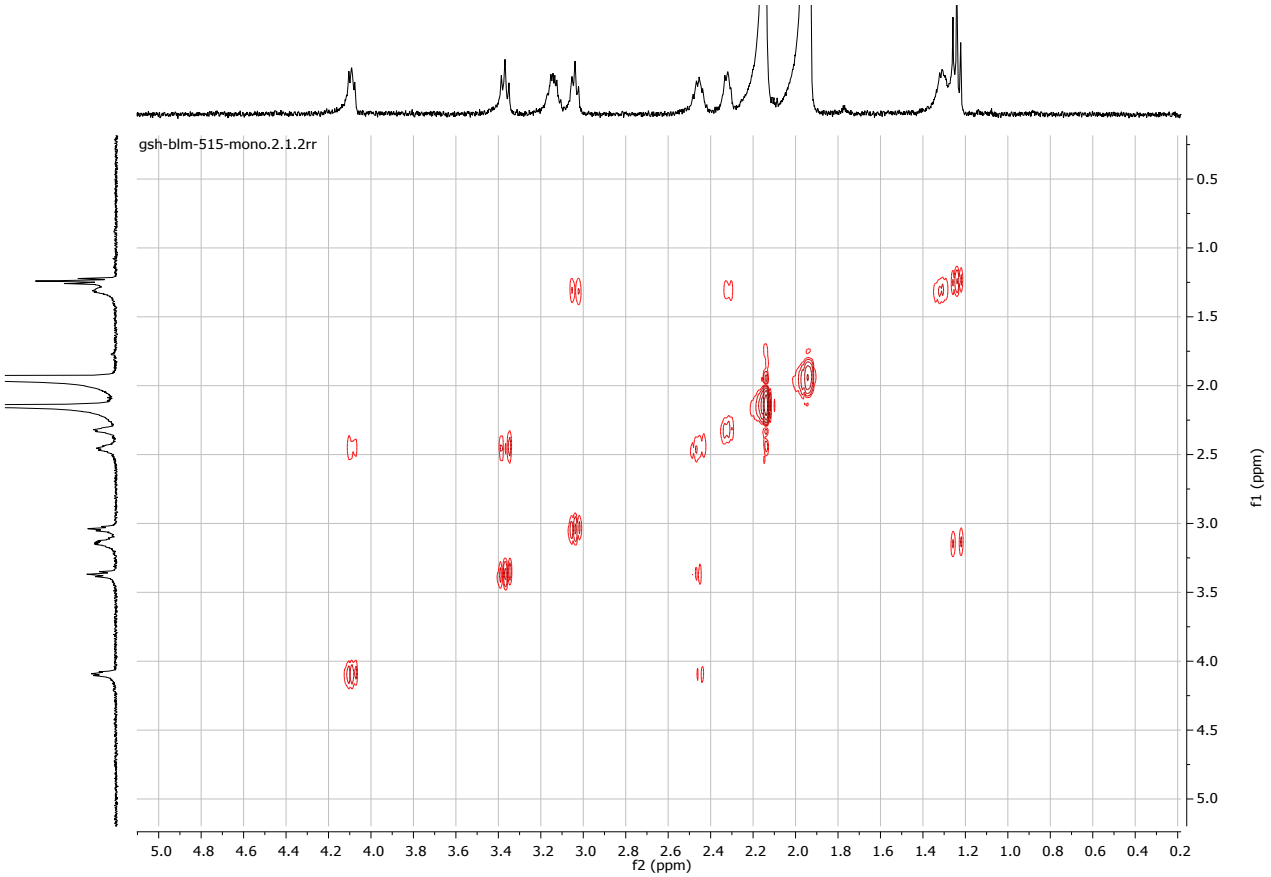

Figure S5. COSY spectra of the aliphatic region of **1** in acetonitrile-d_3.

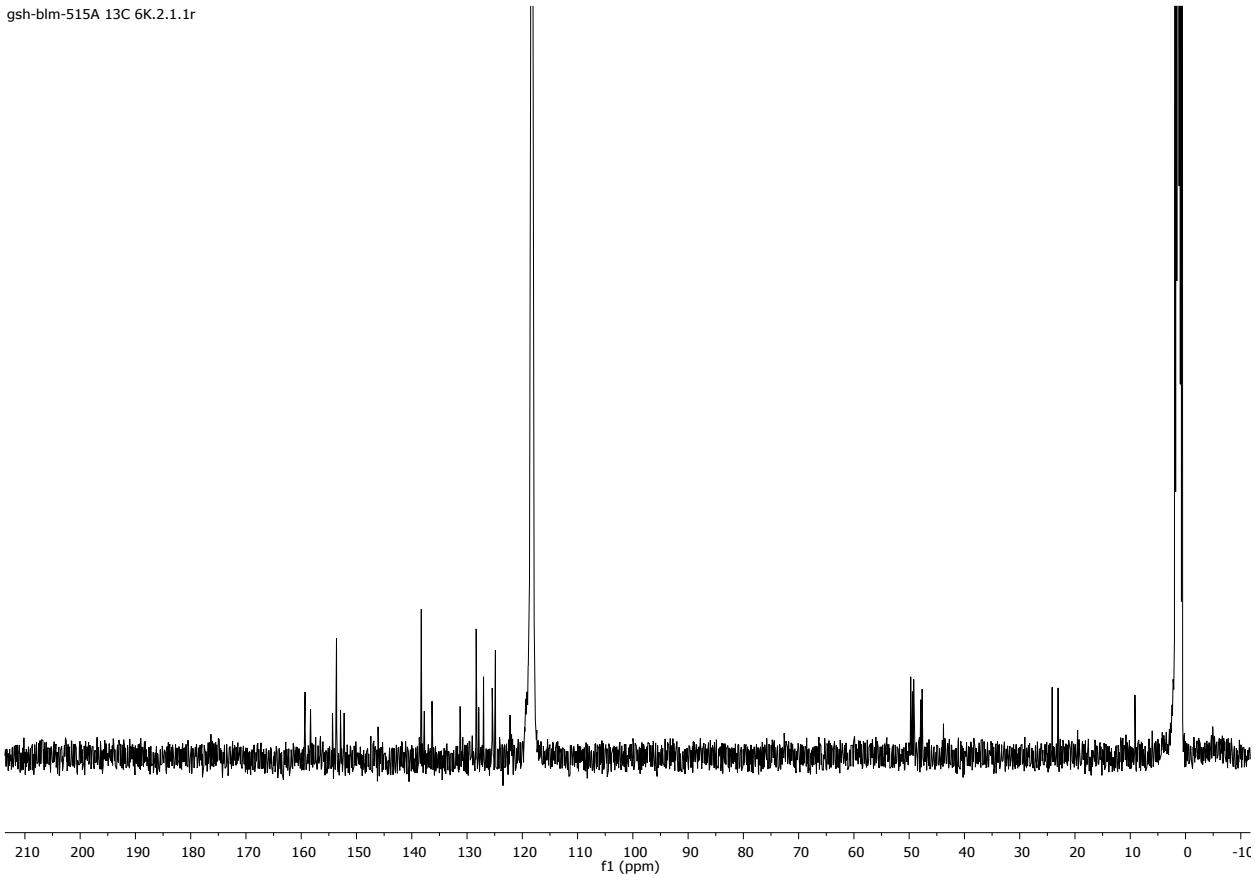

Figure S6. ^{13}C NMR spectra of **1** in acetonitrile-d_3.

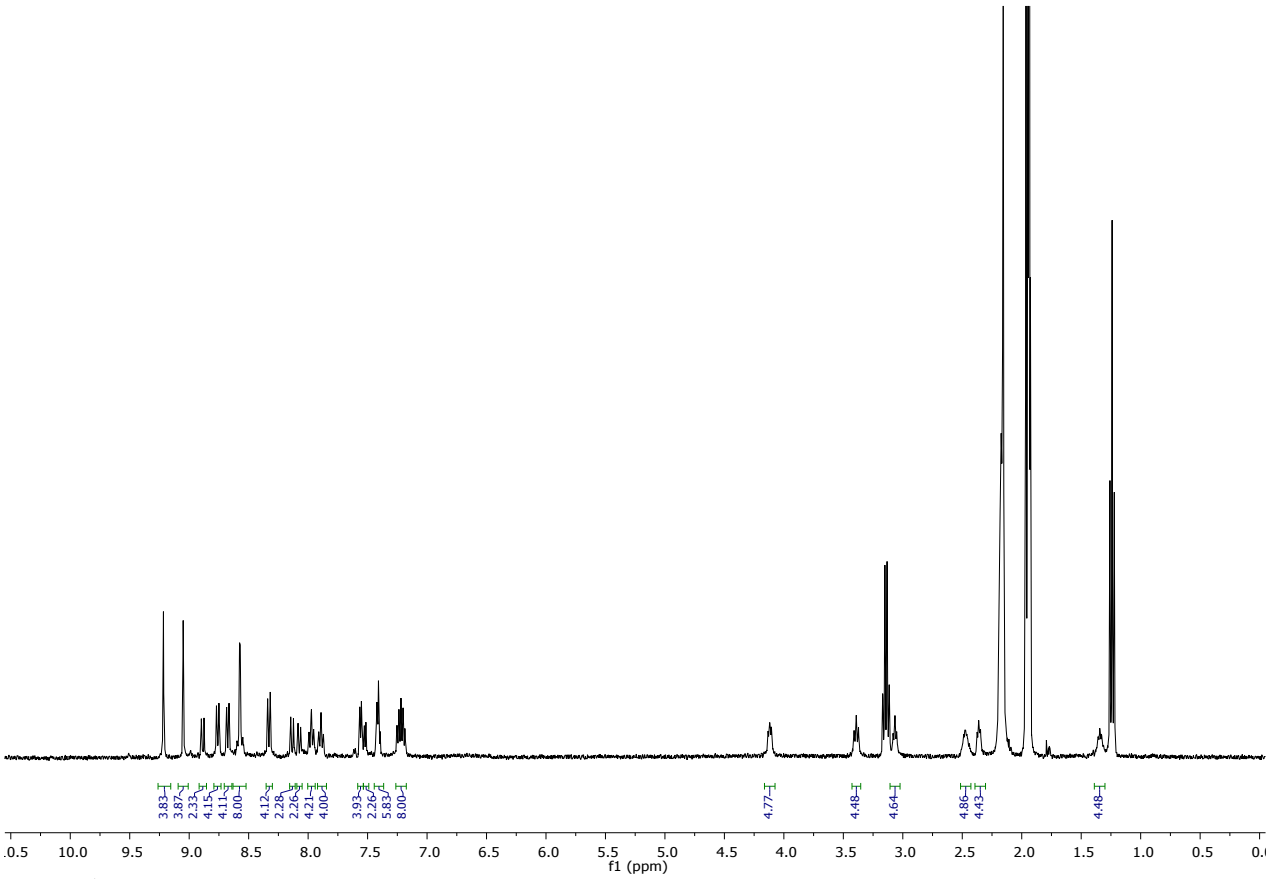

Figure S7. ^{1}H NMR spectra of **2** in acetonitrile-d_3.

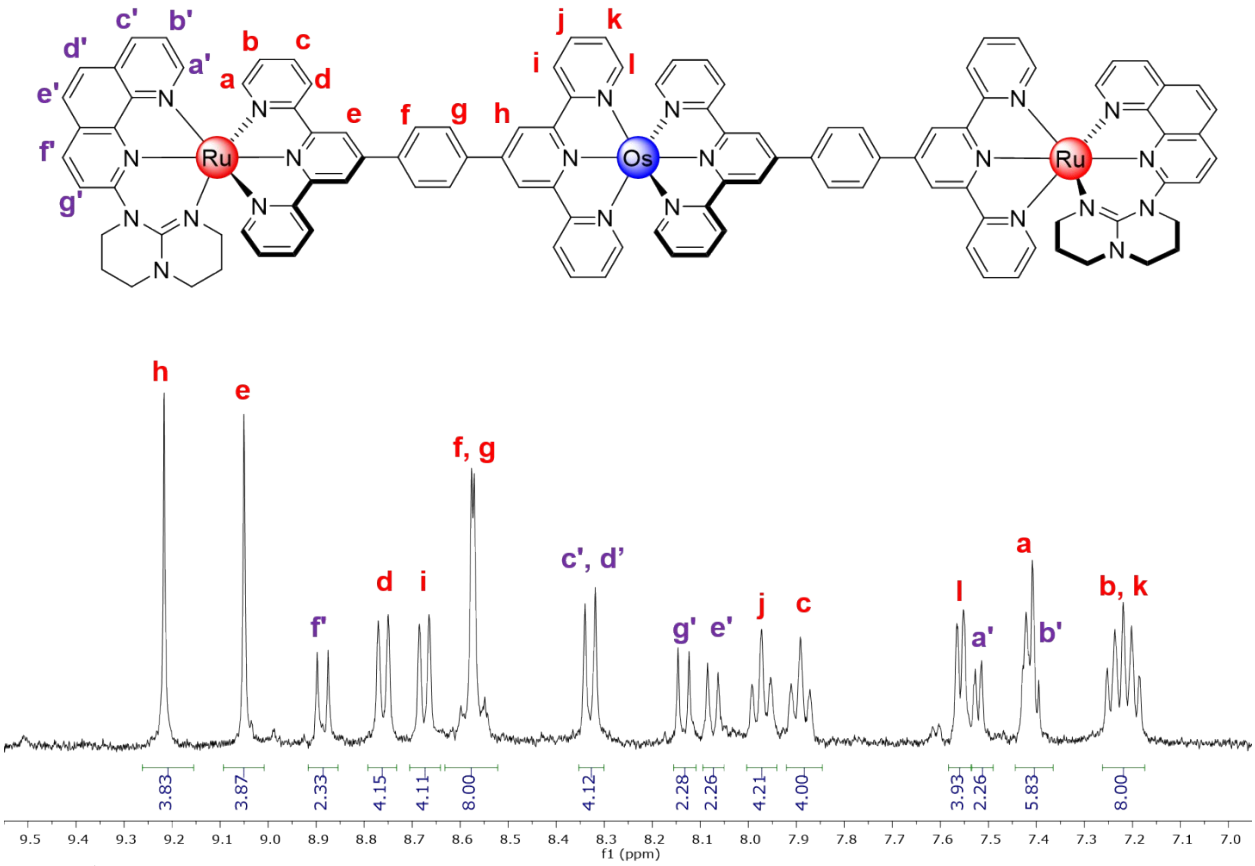

Figure S8. ^{1}H NMR spectra of the aromatic region of **2** in acetonitrile-d_3.

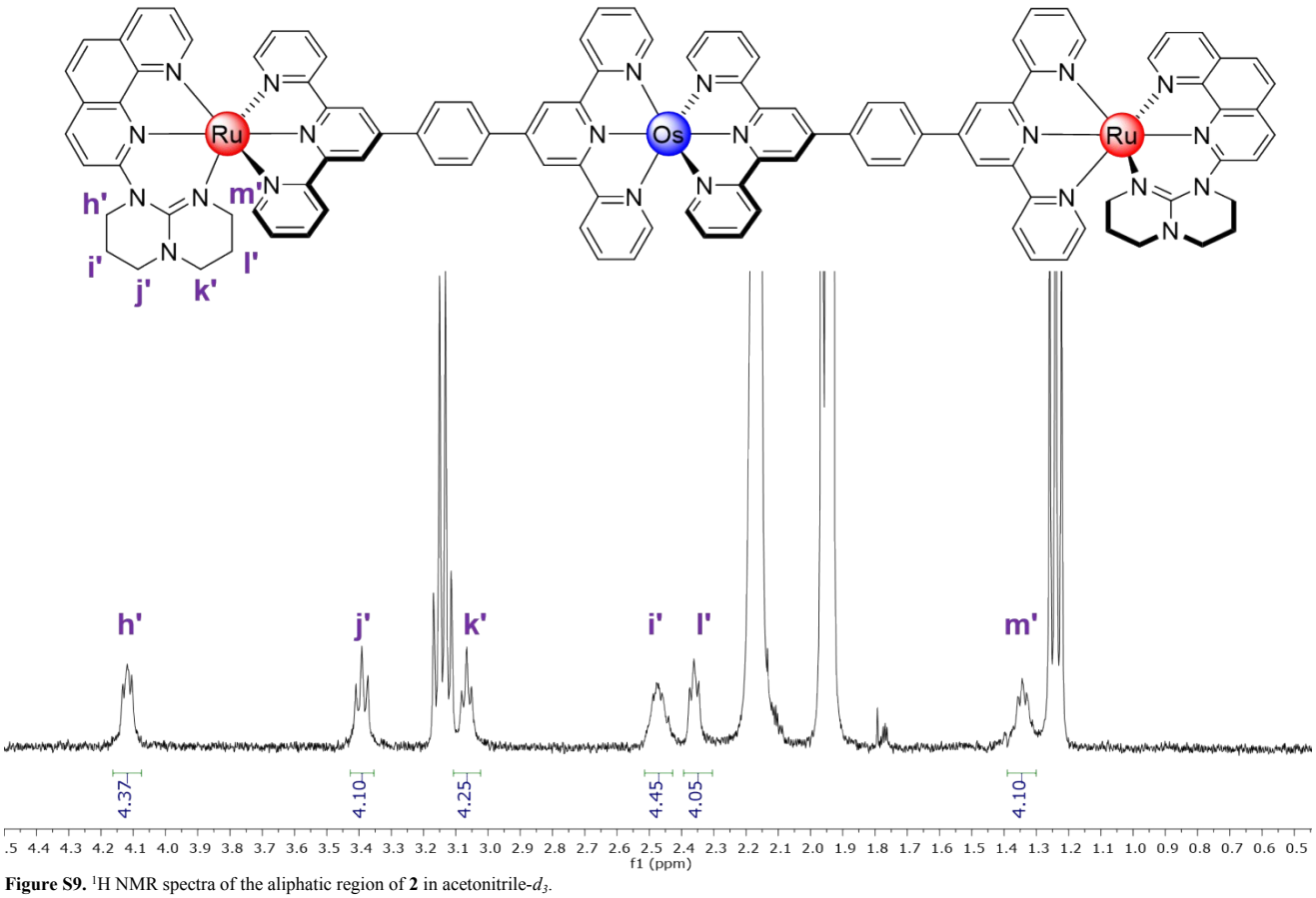

Figure S9. ^{1}H NMR spectra of the aliphatic region of **2** in acetonitrile-d_3.

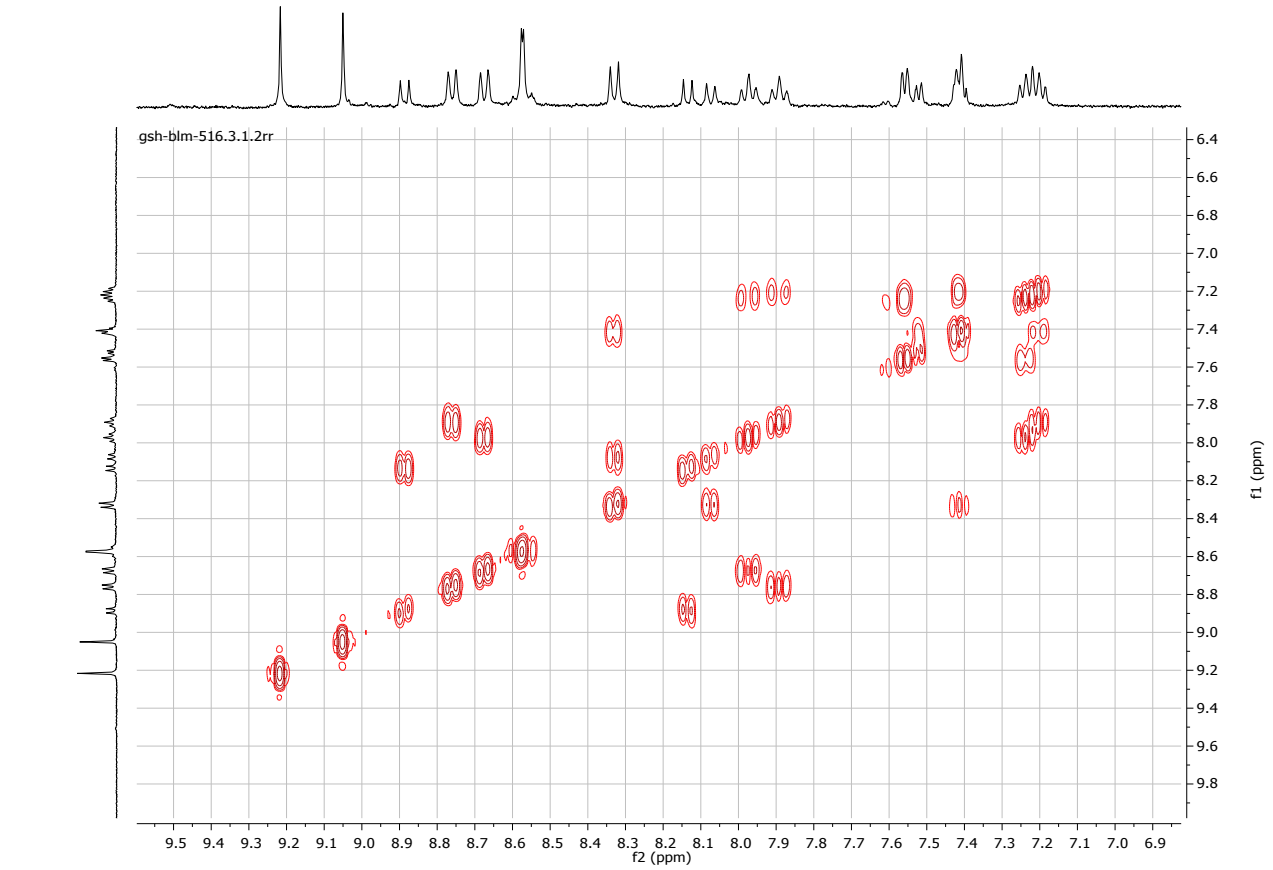

Figure S10. COSY spectra of the aromatic region of **2** in acetonitrile-d_3.

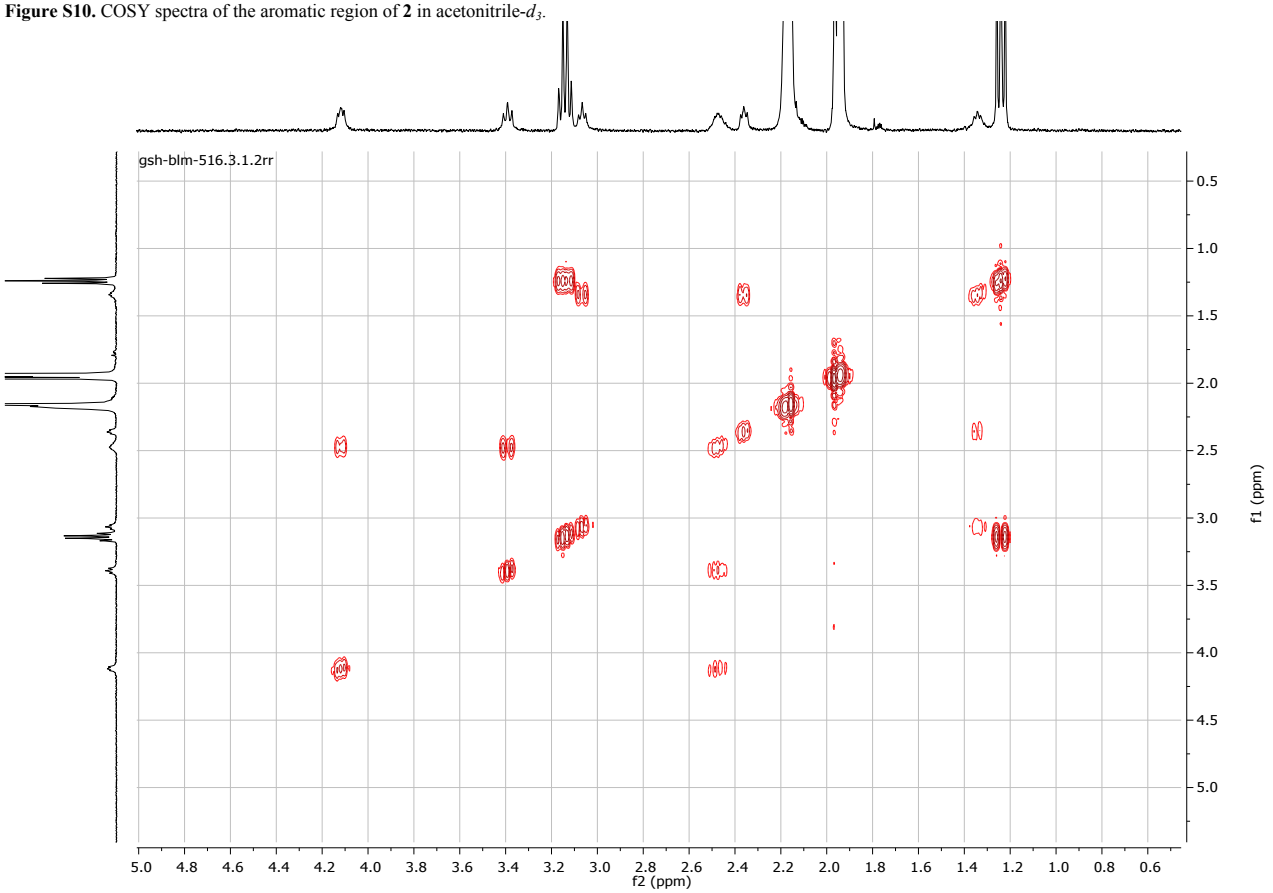

Figure S11. COSY spectra of the aliphatic region of **2** in acetonitrile-d_3.

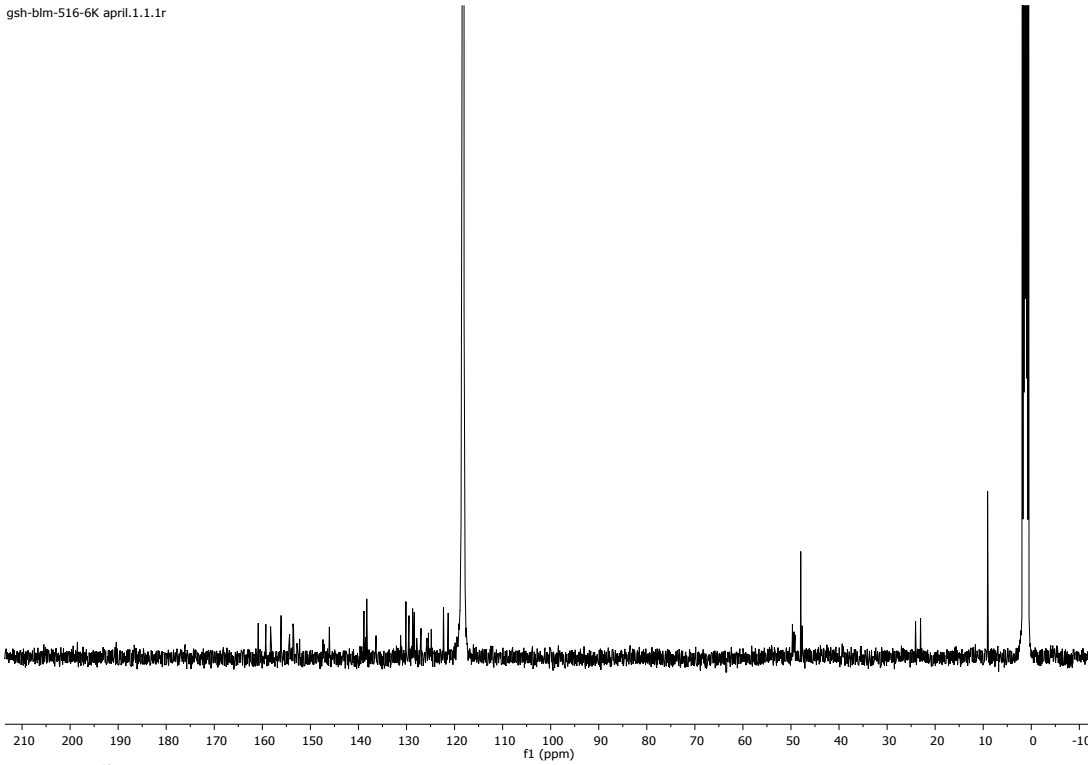

Figure S12. ^{13}C NMR spectra of **2** in acetonitrile-d_3.

Table S1. Solid-state structure and refinement data for complex **1**.

	1
Formula	$[C_{55}H_{43}N_{11}Ru][(PF_6)_2]$
Color/form	Red/block
M_w [gmol^{-1}]	1249.01
Temperature [K]	150.0
Wavelength [Å]	1.341139
Crystal system	Triclinic
a [Å]	9.335(2)
b [Å]	12.808(3)
c [Å]	23.398(5)
α [°]	97.096(4)
β [°]	100.183(5)
γ [°]	92.627(4)
V [Å^3]	2725.9(9)
Space group	*P*-1
Z	2
$d_{calcd.}$ [gcm^{-3}]	1.522
μ [mml^{-1}]	2.422
F(000)	1264
Reflection collected	6455
Independent reflections	2473
GoF	1.076
R_1(F) [$I > 2\sigma(I)$]	0.1470
$wR(F^2)$ [$I > 2\sigma(I)$]	0.3280
R_1(F) (all data)	0.2783
wR(F^2) (all data)	0.4138
Largest diff. peak/hole [eÅ^{-3}]	1.152

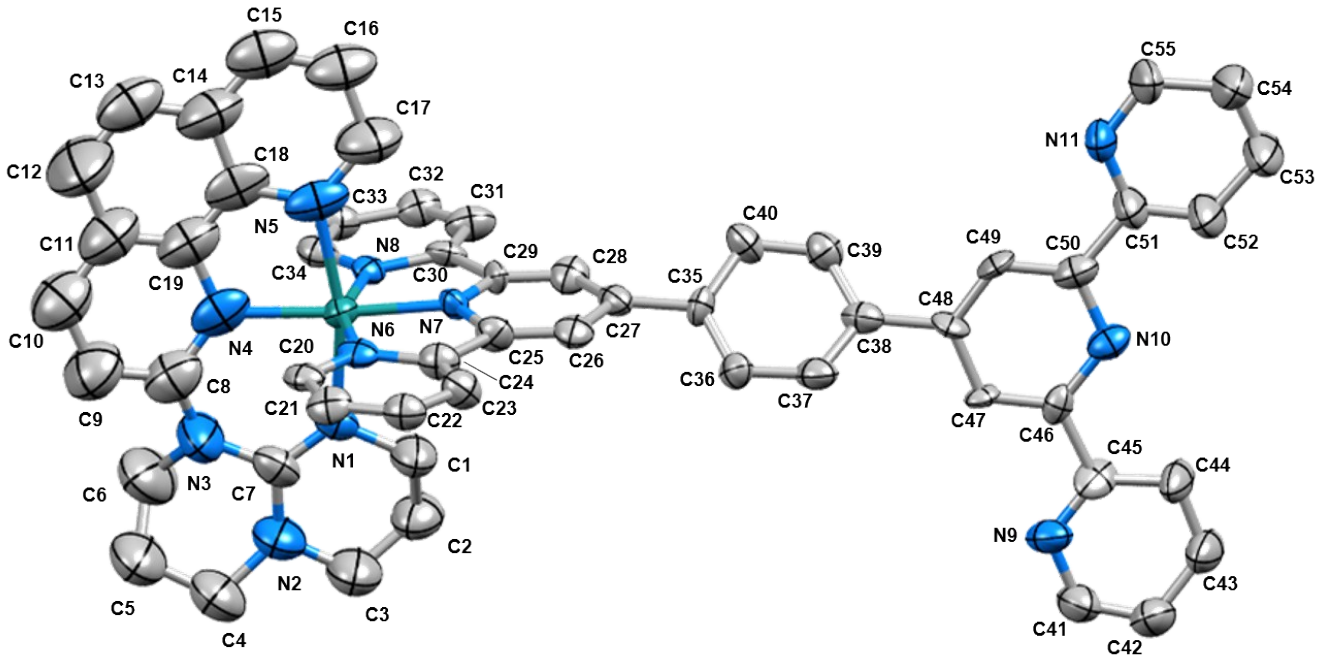

Figure S13. Thermal ellipsoid diagram (30% probability) of X-ray structure of **1** with atoms' numbering. Hydrogen atoms and counter-anions are omitted for clarity.

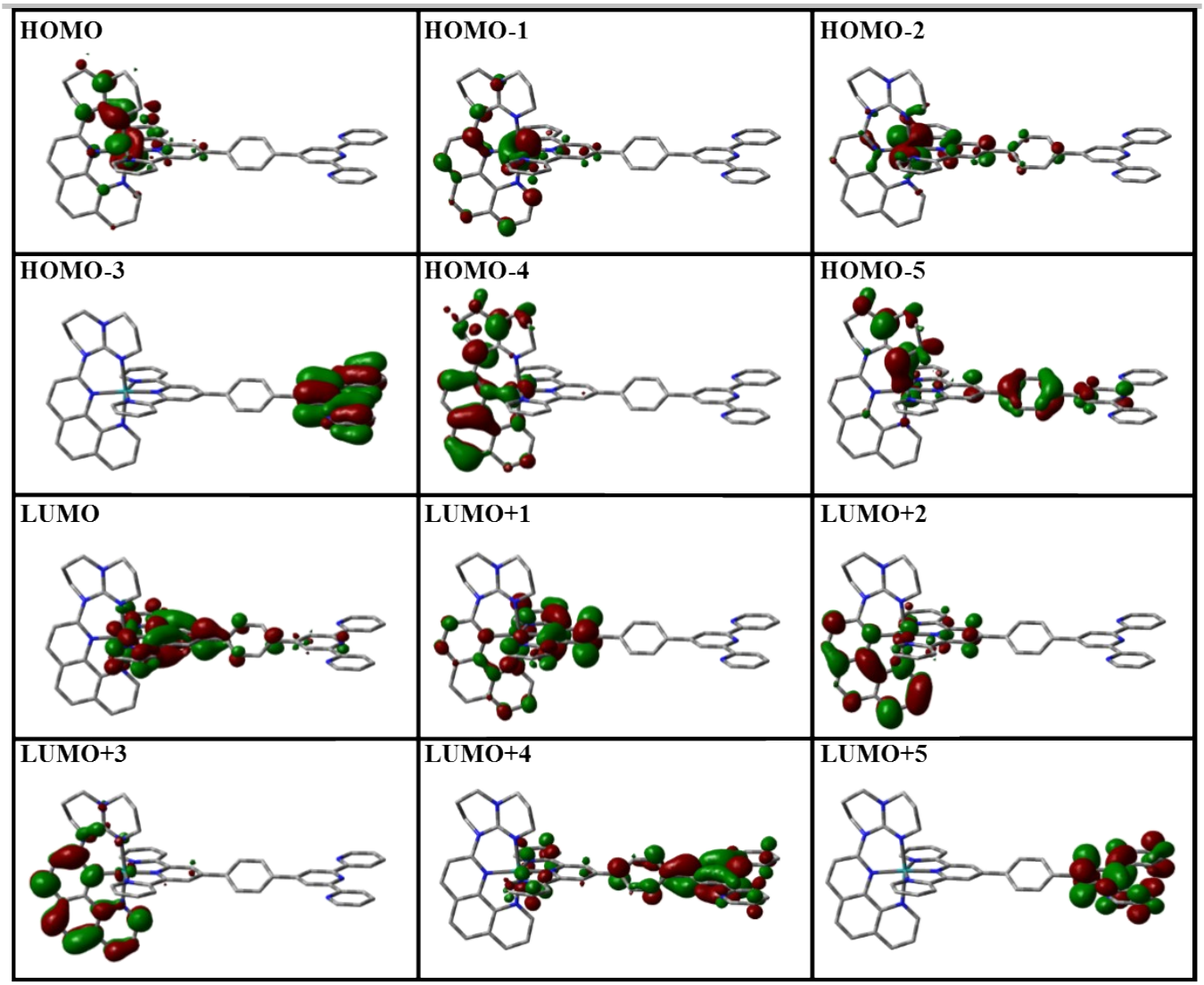

Figure S14. Kohn-Sham electron density illustration of the molecular orbitals for **1** in ($S = 0$) the ground-state.

Table S2. MO composition of **1** in (*S=0*) ground state.

MO	Energy (eV)	Composition (%)		
		Ruthenium	phen-hpp	phenyl-1,4-bistpy
LUMO+5	-1.903	0	0	100
LUMO+4	-2.049	0	0	99
LUMO+3	-2.281	1	94	4
LUMO+2	-2.434	5	77	18
LUMO+1	-2.529	1	20	79
LUMO	**-2.773**	**8**	**3**	**89**
HOMO	**-5.843**	**55**	**32**	**13**
HOMO-1	-6.256	62	24	14
HOMO-2	-6.409	71	8	21
HOMO-3	-7.016	0	0	100
HOMO-4	-7.211	9	86	5
HOMO-5	-7.230	9	50	41

Table S3 - Selected transitions from TD-DFT calculations of **1** in the singlet ground state (PBE0), CPCM (CH_3CN).

Energy (eV)	λ (nm)	f	Transition	Character
2.01	615	0.0269	H→L (90%)	$^1MLCT_{Ru\rightarrow bistpy}$ (maj.) + $LLCT_{phen\text{-}hpp\rightarrow bistpy}$
2.35	525	0.0096	H-1→L (58%), H→L+1 (10%), H→L+2 (15%)	$^1MLCT_{Ru\rightarrow bistpy}$
2.38	518	0.0072	H-1→L (21%), H→L+1 (24%), H→L+2 (42%)	$^1MLCT_{Ru\rightarrow bistpy}$ (maj.) + $^1MLCT_{Ru\rightarrow phen\text{-}hpp}$
2.41	512	0.0148	H→L+1 (57%), H→L+2 (30%)	
2.67	463	0.2461	H-2→L (51%), H-1→L+2 (19%)	
2.68	461	0.0021	H→L+3 (91%)	$^1MLCT_{Ru\rightarrow phen\text{-}hpp}$
2.81	440	0.1574	H-1→L+1 (88%)	$^1MLCT_{Ru\rightarrow bistpy}$
2.86	431	0.0124	H-2→L+1 (14%), H-2→L+2 (75%)	$^1MLCT_{Ru\rightarrow phen\text{-}hpp}$
2.89	427	0.0216	H-2→L+1 (80%), H-2→L+2 (13%)	$^1MLCT_{Ru\rightarrow bistpy}$ + $^1MLCT_{Ru\rightarrow phen\text{-}hpp}$
3.04	406	0.0726	H-1→L+2 (63%)	
3.15	392	0.0414	H-2→L+3 (10%), H-1→L+3 (82%)	$^1MLCT_{Ru\rightarrow phen\text{-}hpp}$
3.23	382	0.0644	H-2→L+3 (72%)	
3.25	379	0.0828	H→L+4 (65%), H→L+6 (18%)	$^1MLCT_{Ru\rightarrow bistpy}$ (maj.) + $LLCT_{phen\text{-}hpp\rightarrow bistpy}$
3.48	354	0.0049	H→L+6 (25%), H→L+7 (45%)	
3.64	339	0.1138	H-1→L+4 (60%), H-1→L+6 (25%)	
3.64	339	0.0011	H→L+5 (98%)	
3.67	336	0.1212	H-6→L (11%), H-5→L (72%)	
3.73	331	0.3066	H-4→L (16%), H-2→L+4 (53%), H-2→L+6 (19%)	$LLCT_{phen\text{-}hpp\rightarrow bistpy}$
3.92	315	0.1647	H-6→L (15%), H-2→L+6 (12%), H-2→L+7 (44%) H-1→L+6 (11%)	$^1MLCT_{Ru\rightarrow bistpy}$ (maj.) + $LLCT_{phen\text{-}hpp\rightarrow bistpy}$
3.94	313	0.2598	H-6→L (32%), H-2→L+7 (10%), H→L+9 (14%)	
4.12	300	0.1486	H-4→L+1 (19%), H-4→L+3 (34%)	
4.14	298	0.1681	H-9→L (25%), H-6→L+1 (14%)	
4.21	293	0.1300	H-9→L (29%), H-6→L+1 (46%)	$^1MLCT_{Ru\rightarrow bistpy}$
4.25	290	0.1712	H-3→L+4 (56%), H-2→L+5 (21%)	$^1MLCT_{Ru\rightarrow bistpy}$ + $LLCT_{phen\text{-}hpp\rightarrow bistpy}$
4.48	275	0.1691	H-3→L+3 (75%), H-3→L+5 (16%)	$^1MLCT_{Ru\rightarrow bistpy}$
4.49	275	0.5137	H-9→L+1 (15%), H-3→L+3 (24%), H-3→L+5 (47%)	$LLCT_{bistpy\rightarrow phen\text{-}hpp}$
4.59	269	0.1134	H-10→L (37%), H-9→L+2 (12%)	
4.61	268	0.0963	H-9→L+1 (10%), H-2→L+8 (16%), H-2→L+15 (11%)	$^1MLCT_{Ru\rightarrow bistpy}$
4.71	262	0.0816	H→L+13 (48%)	$^1MLCT_{Ru\rightarrow phen\text{-}hpp}$
4.72	262	0.4052	H-6→L+5 (33%), H-5→L+5 (36%)	$^1MLCT_{Ru\rightarrow bistpy}$ + $LLCT_{phen\text{-}hpp\rightarrow bistpy}$ (maj.)
5.24	236	0.1091	H-17→L+1 (21%), H-12→L+4 (12%), H-2→L+11 (13%) H-2→L+12 (30%)	$^1MLCT_{Ru\rightarrow bistpy}$
5.27	234	0.1147	H→L+17 (46%)	$^1MLCT_{Ru\rightarrow bistpy}$ + $^1MLCT_{Ru\rightarrow phen\text{-}hpp}$
5.41	228	0.2714	H-14→L+3 (49%)	$^1MLCT_{Ru\rightarrow bistpy}$
5.43	227	0.0857	H-16→L (13%), H-5→L+8 (41%)	$LLCT_{phen\text{-}hpp\rightarrow bistpy}$
5.46	226	0.0909	H-9→L+6 (18%), H-9→L+7 (14%), H-5→L+8 (11%)	
5.49	225	0.2332	H-4→L+8 (26%), H-4→L+9 (28%)	
5.53	223	0.1065	H-5→L+9 (11%), H-4→L+8 (16%), H-4→L+9 (15%) H-2→L+14 (24%)	
5.73	216	0.0898	H-15→L+4 (39%), H-3→L+9 (12%)	$LLCT_{bistpy\rightarrow phen\text{-}hpp}$

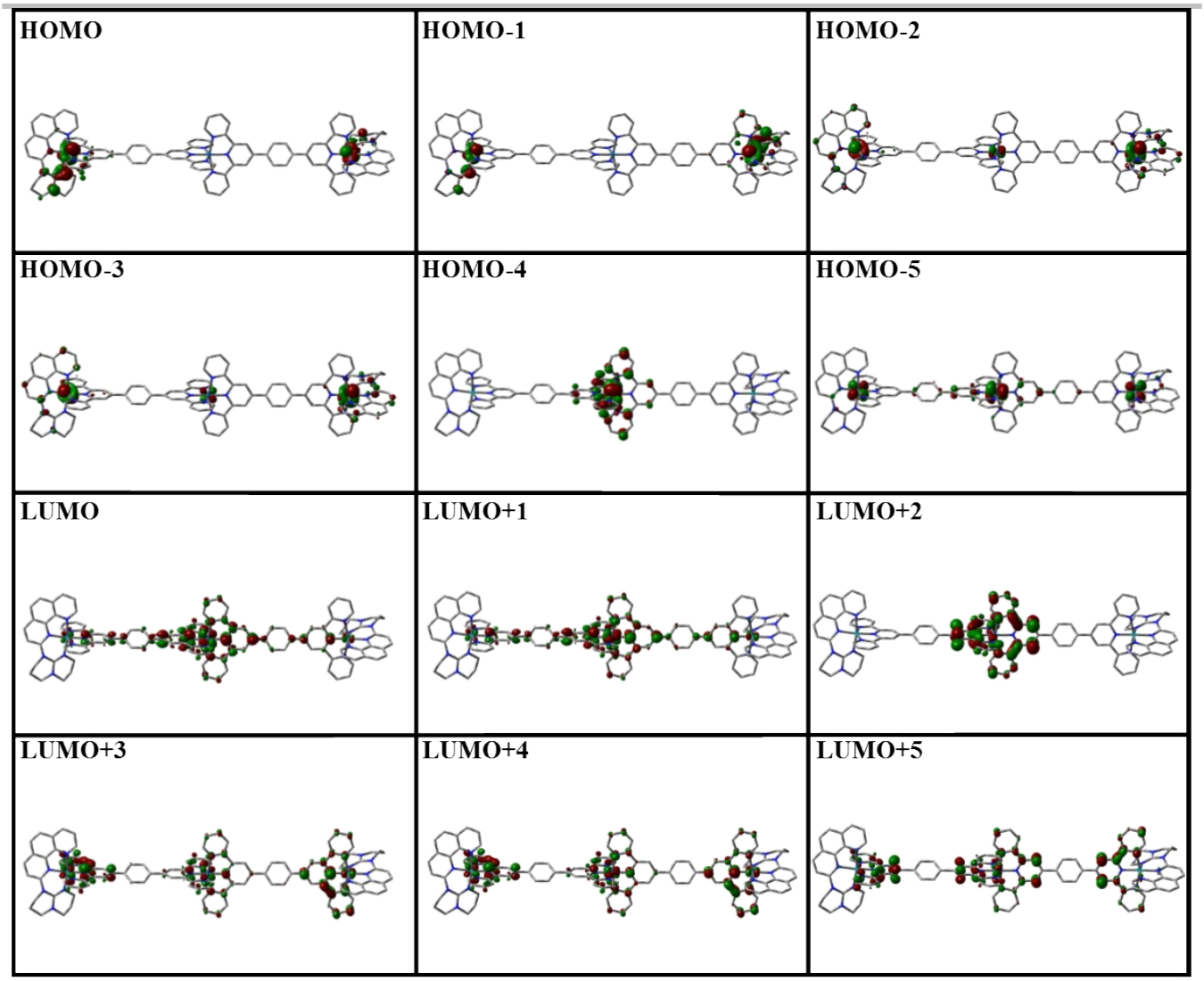

Figure S15. Kohn-Sham electron density illustration of the molecular orbitals for **2** in ($S = 0$) the ground-state.

Table S4. MO composition of **2** in (*S=0*) ground state.

MO	Energy (eV)	Composition (%)			
		Ruthenium	Osmium	phen-hpp	phenyl-1,4-bistpy
LUMO+5	-2.628	1	2	8	89
LUMO+4	-2.770	5	3	3	89
LUMO+3	-2.775	5	3	3	89
LUMO+2	-2.807	0	0	0	100
LUMO+1	-3.042	3	9	1	87
LUMO	**-3.056**	**3**	**9**	**1**	**87**
HOMO	**-5.930**	**55**	**0**	**32**	**13**
HOMO-1	-5.930	55	0	32	13
HOMO-2	-6.337	57	4	21	17
HOMO-3	-6.337	58	4	22	17
HOMO-4	-6.395	0	61	0	39
HOMO-5	-6.435	37	27	7	29

Table S5 - Selected transitions from TD-DFT calculations of **2** in the singlet ground state (PBE0), CPCM (CH_3CN).

Energy (eV)	λ (nm)	f	Transition	Character
1.98	624	0.0677	H-1→L+1 (22%), H-1→L+4 (23%), H→L (21%) H→L+3 (24%)	$^1MLCT_{Ru\rightarrow bistpy}$ (maj.) + $LLCT_{phen\text{-}hpp\rightarrow bistpy}$
1.98	624	0.0078	H-1→L (21%), H-1→L+3 (24%), H→L+1 (22%) H→L+4 (23%)	
2.26	547	0.0194	H-4→L (80%), H-4→L+3 (18%)	$^1MLCT_{Os\rightarrow bistpy}$
2.27	544	0.0192	H-4→L+1 (78%), H-4→L+4 (20%)	
2.31	535	0.0011	H-8→L (15%), H-7→L+1 (14%), H-6→L+1 (19%) H-5→L (21%)	$^1MLCT_{Ru\rightarrow bistpy}$ (maj.) + $^1MLCT_{Os\rightarrow bistpy}$ + $LLCT_{phen\text{-}hpp\rightarrow bistpy}$
2.33	531	0.0223	H-3→L+1 (17%), H-3→L+4 (17%), H-2→L (16%) H-2→L+3 (18%)	$^1MLCT_{Ru\rightarrow bistpy}$ (maj.) + $LLCT_{phen\text{-}hpp\rightarrow bistpy}$
2.33	530	0.0043	H-3→L (15%), H-3→L+3 (18%), H-2→L+1 (16%) H-2→L+4 (17%)	
2.39	517	0.0152	H-1→L+6 (18%), H→L+5 (15%), H→L+6 (11%) H→L+7 (10%), H→L+9 (16%)	$^1MLCT_{Ru\rightarrow bistpy}$
2.39	517	0.0048	H-1→L+5 (15%), H-1→L+6 (11%), H-1→L+7 (10%) H-1→L+8 (10%), H→L+6 (18%), H→L+8 (11%)	
2.40	514	0.0075	H-1→L+6 (13%), H-1→L+8 (28%), H→L+9 (28%)	$^1MLCT_{Ru\rightarrow phen\text{-}hpp}$ + $^1MLCT_{Ru\rightarrow bistpy}$
2.40	514	0.0185	H-1→L+9 (23%), H→L+6 (14%), H→L+8 (23%)	
2.42	511	0.0000	H-8→L+1 (13%), H-7→L (15%), H-6→L (21%) H-5→L+1 (18%)	$^1MLCT_{Ru\rightarrow bistpy}$ (maj.) + $^1MLCT_{Os\rightarrow bistpy}$ + $LLCT_{phen\text{-}hpp\rightarrow bistpy}$
2.50	494	1.0919	H-6→L+1 (24%), H-5→L (22%)	
2.65	466	0.3917	H-8→L (11%), H-7→L+1 (10%), H-4→L+2 (20%)	$^1MLCT_{Ru\rightarrow bistpy}$ + $^1MLCT_{Os\rightarrow bistpy}$
2.77	446	0.6177	H-4→L+2 (53%), H-3→L+6 (12%)	
3.04	406	0.1099	H-3→L+8 (28%), H-2→L+9 (27%)	$^1MLCT_{Ru\rightarrow bistpy\ and/or\ phen\text{-}hpp}$ (maj.) + $^1MLCT_{Os\rightarrow bistpy\ and/or\ phen\text{-}hpp}$
3.25	380	0.1207	H-7→L+1 (16%), H-6→L+1 (10%), H-6→L+10 (10%) H-5→L+11 (10%)	
3.28	376	0.4063	H-8→L+3 (25%), H-7→L+4 (30%), H-6→L+1 (12%)	$^1MLCT_{Ru\rightarrow bistpy}$ + $^1MLCT_{Os\rightarrow bistpy}$
3.71	333	0.2004	H-3→L+12 (25%), H-2→L+13 (26%)	$^1MLCT_{Ru\rightarrow bistpy}$ (maj.) + $^1MLCT_{Os\rightarrow bistpy}$ + $LLCT_{phen\text{-}hpp\rightarrow bistpy}$
3.74	330	0.2351	H-6→L+12 (27%), H-5→L+13 (27%)	
3.85	320	0.1011	H-8→L+13 (16%), H-7→L+12 (16%), H-6→L+16 (16%) H-5→L+15 (16%)	
4.00	309	0.1520	H-11→L+6 (15%)	$^1MLCT_{Ru\rightarrow bistpy}$ (maj.) + $LLCT_{phen\text{-}hpp\rightarrow bistpy}$
4.01	308	0.1487	H-3→L+12 (13%), H-3→L+20 (17%), H-2→L+13 (12%) H-2→L+19 (17%)	
4.05	305	0.1465	H-17→L (23%), H-4→L+12 (23%), H-4→L+16 (17%)	$^1MLCT_{Os\rightarrow bistpy}$
4.05	305	0.1378	H-17→L+1 (17%), H-4→L+13 (24%), H-4→L+15 (20%)	
4.08	302	0.4324	H-12→L (13%)	$^1MLCT_{Ru\rightarrow bistpy}$ + $LLCT_{phen\text{-}hpp\rightarrow bistpy}$ (maj.)
4.10	301	0.1553	H-12→L+8 (11%), H-11→L+9 (11%)	
4.12	299	0.2888	H-17→L (43%), H-4→L+16 (29%)	$^1MLCT_{Os\rightarrow bistpy}$
4.13	299	0.3700	H-17→L+1 (41%), H-4→L+15 (26%)	
4.13	299	0.1560	H-6→L+20 (11%), H-5→L+19 (11%)	$^1MLCT_{Ru\rightarrow bistpy}$ + $^1MLCT_{Os\rightarrow bistpy}$ + $LLCT_{phen\text{-}hpp\rightarrow bistpy}$
4.20	294	0.4041	H-16→L (25%), H-15→L+1 (22%)	$^1MLCT_{Ru\rightarrow bistpy}$ + $LLCT_{phen\text{-}hpp\rightarrow bistpy}$ (maj.)
4.47	276	0.1589	H-20→L+2 (11%), H-16→L+3 (31%), H-15→L+4 (35%)	$LLCT_{bistpy\rightarrow phen\text{-}hpp}$
4.50	274	0.1120	H-20→L+2 (46%), H-14→L (20%)	
4.56	271	0.1003	H-15→L+6 (15%), H-14→L+9 (10%), H-13→L+8 (10%)	
4.60	268	0.2927	H-17→L+5 (10%), H-17→L+7 (15%), H-14→L+9 (10%) H-13→L+8 (10%)	$^1MLCT_{Ru\rightarrow phen\text{-}hpp}$ + $^1MLCT_{Os\rightarrow phen\text{-}hpp}$
4.60	268	0.1176	H-2→L+17 (12%)	$^1MLCT_{Ru\rightarrow bistpy}$ (maj.) + $^1MLCT_{Os\rightarrow bistpy}$
4.66	265	0.1370	H-8→L+17 (12%), H-7→L+18 (12%)	$^1MLCT_{Ru\rightarrow bistpy}$ (maj.) + $^1MLCT_{Os\rightarrow bistpy}$ + $LLCT_{phen\text{-}hpp\rightarrow bistpy}$
4.66	265	0.1649	H-19→L+5 (10%), H-18→L+6 (17%)	$^1MLCT_{Ru\rightarrow bistpy}$ + $^1MLCT_{Os\rightarrow bistpy}$ + $LLCT_{phen\text{-}hpp\rightarrow bistpy}$ (maj.)
4.76	260	0.1184	H-19→L+11 (12%), H-18→L+10 (14%), H-13→L+10 (10%)	$^1MLCT_{Ru\rightarrow phen\text{-}hpp}$ + $LLCT_{bistpy\rightarrow phen\text{-}hpp}$ (maj.)

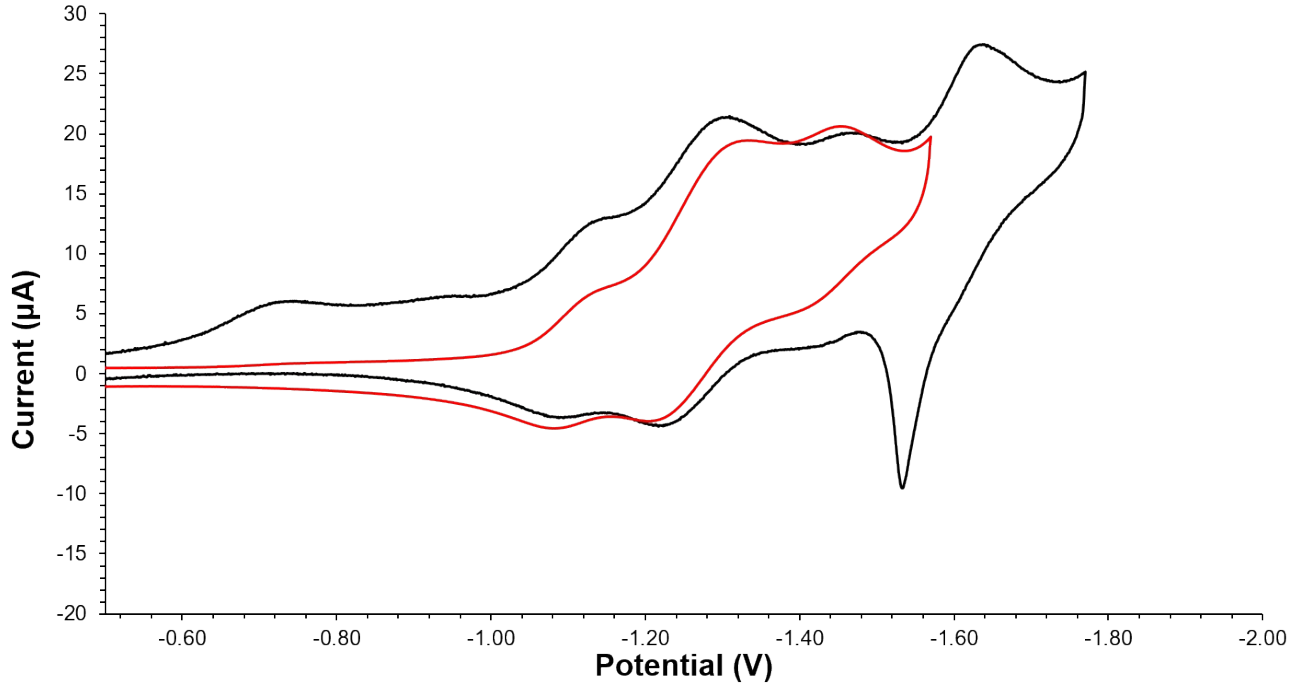

Figure S16. Comparison of the reduction waves of **2** when cycling up to -1.55 V (red) and -1.75 V (black). The three first processes are fully reversible while the fourth one led to adsorption and stripping at the electrode.

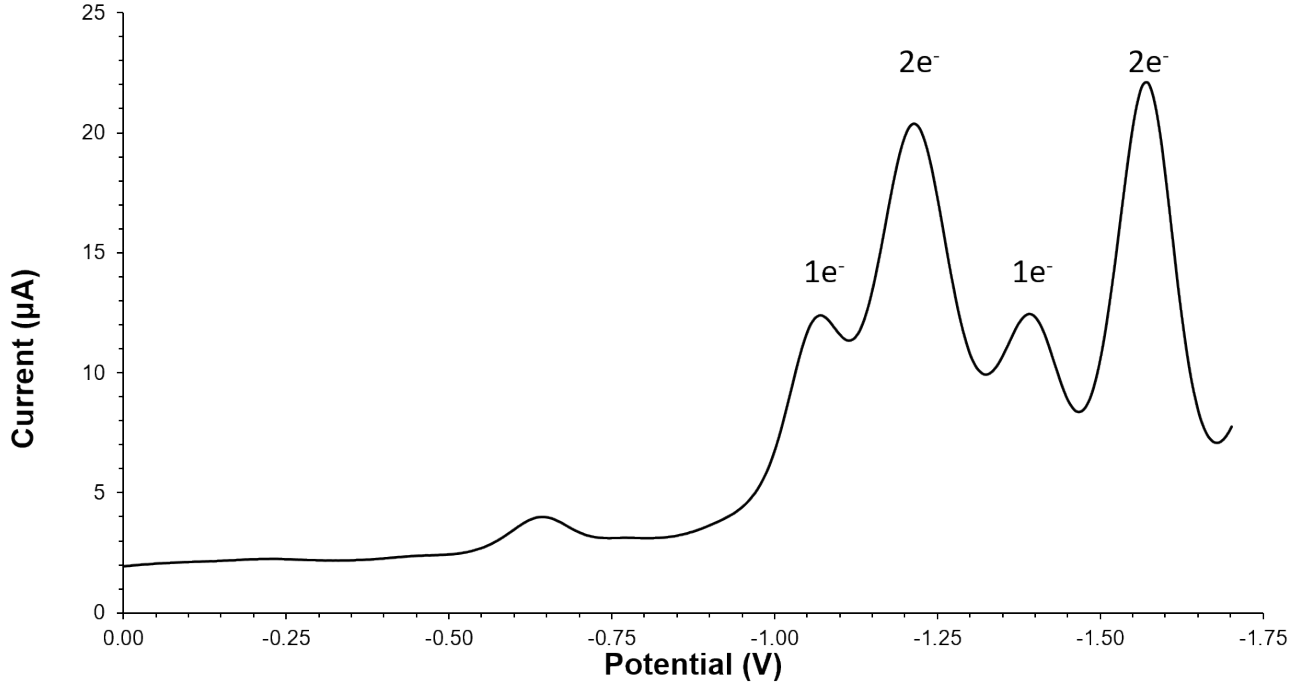

Figure S17. Square-wave voltammetry experiment on **2** displaying the number of electron exchanged during the processes.

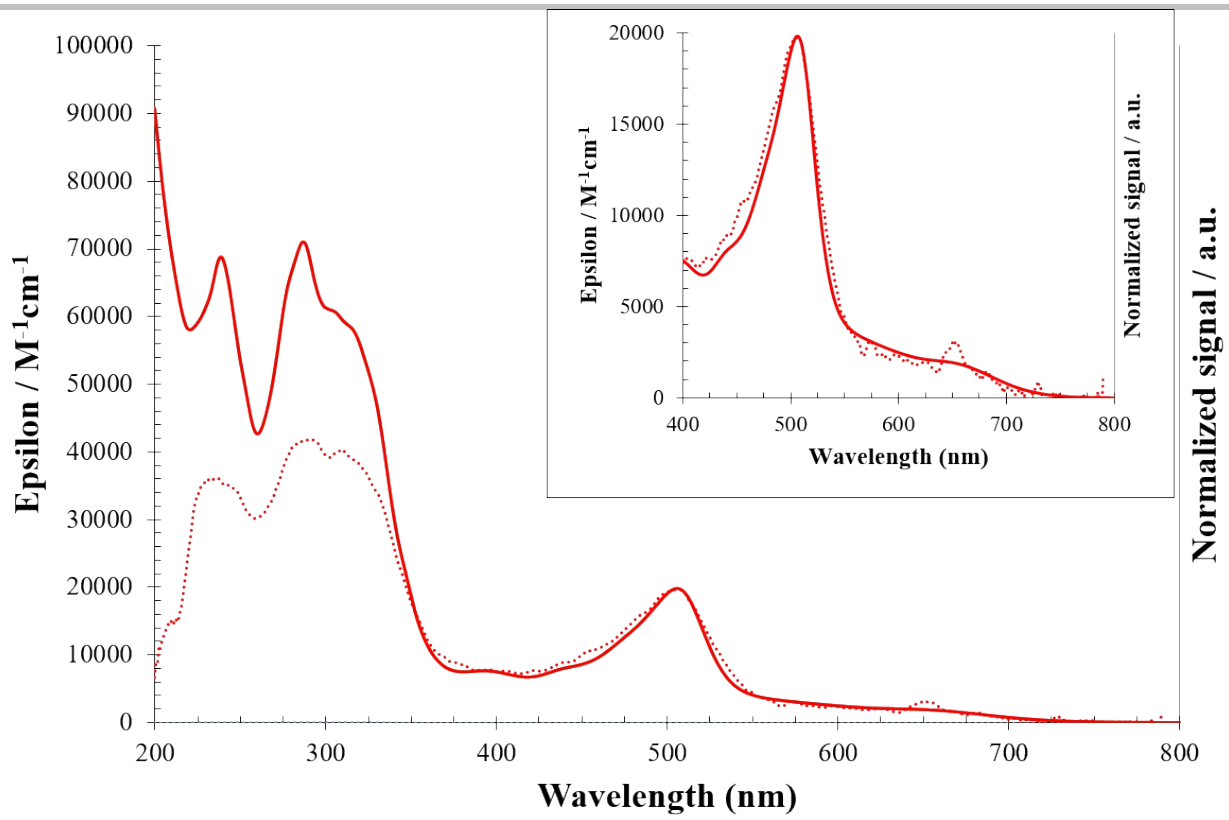

Figure S18. Absorption (plain) and excitation (dots) spectra of **1** in spectrograde acetonitrile solution. The excitation spectrum was recorded with λ_{em} = 805 nm.

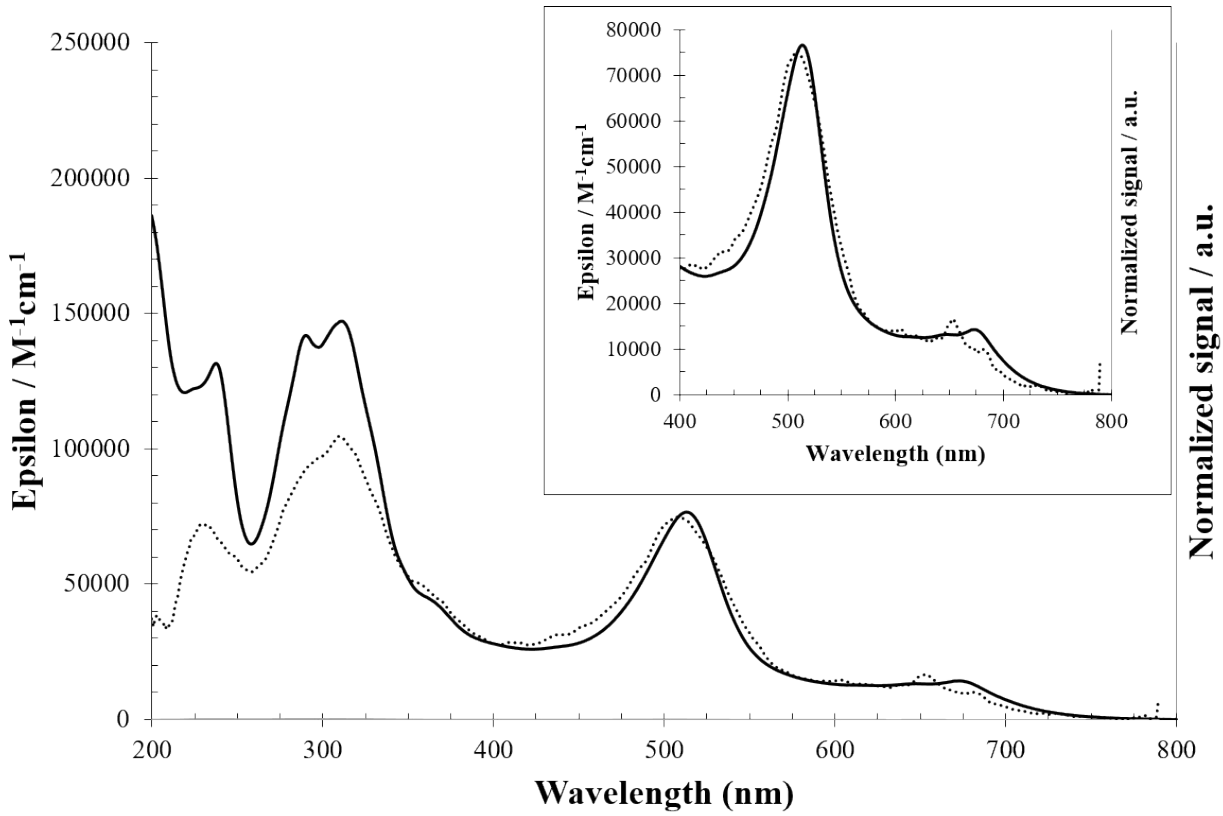

Figure S19. Absorption (plain) and excitation (dots) spectra of **2** in spectrograde acetonitrile solution. The excitation spectrum was recorded with λ_{em} = 805 nm.

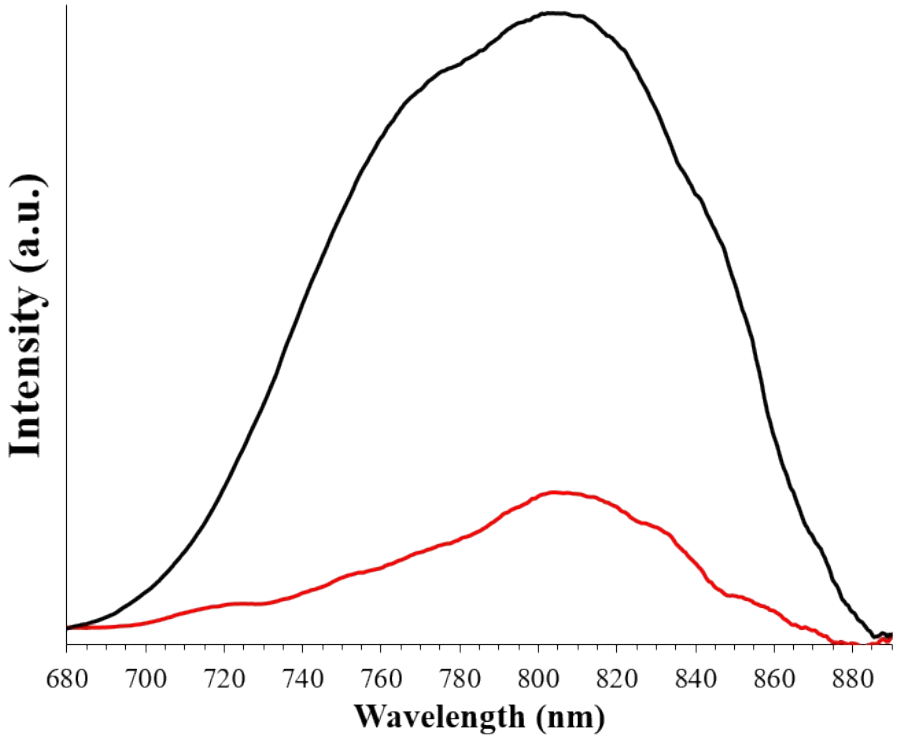

Figure S20. Luminescence spectra of **1** (red) and **2** (black) in deaerated acetonitrile solution at ambient temperature (λex. = 650 nm).

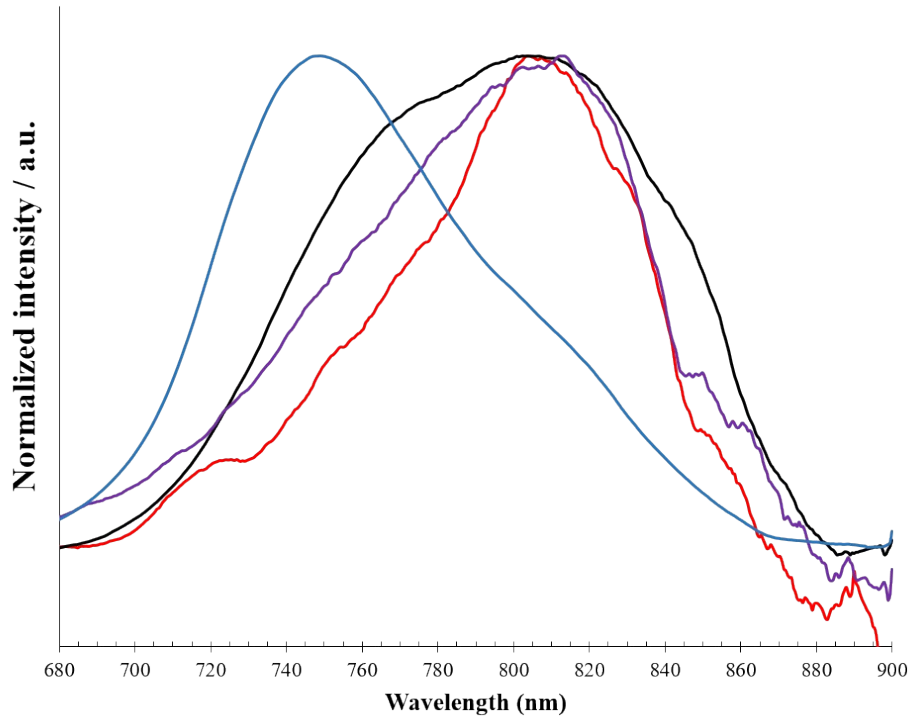

Figure S21. Normalized luminescence spectra of $\mathbf{1}^{2+}$ (red) and $\mathbf{2}^{6+}$ (black), $[\mathbf{Os(ttpy)_2}]^{2+}$ (blue) and $[\mathbf{Ru(phtpy)(phen\text{-}hpp)}]^{2+}$ (purple) recorded in deaerated acetonitrile solution at ambient temperature (λex. = 650 nm).

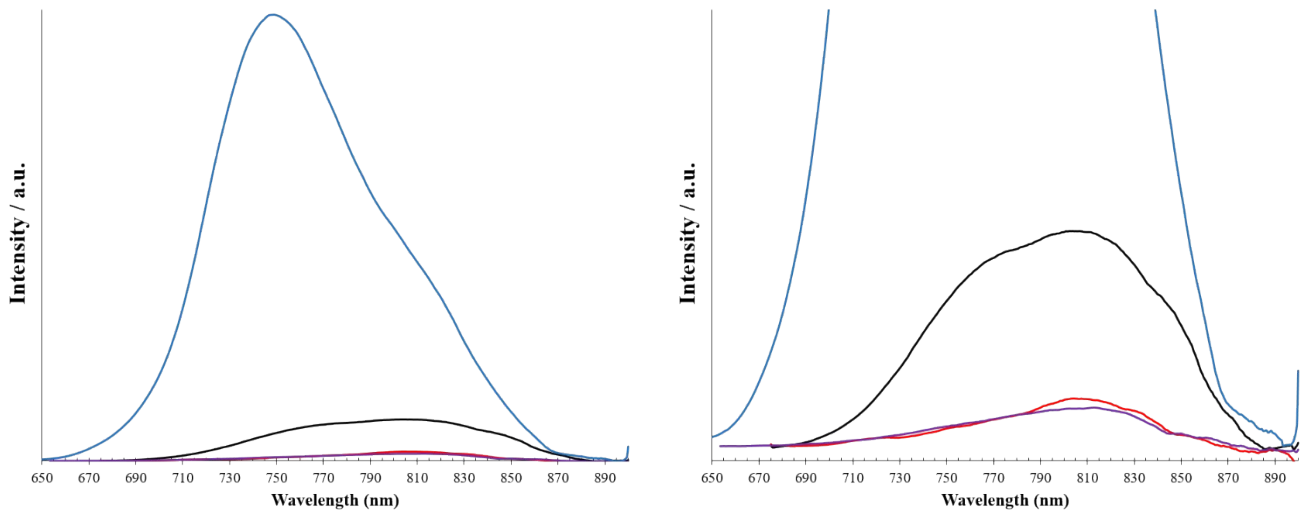

Figure S22. Luminescence spectra of $\mathbf{1}^{2+}$ (red) and $\mathbf{2}^{6+}$ (black), $[\mathbf{Os(ttpy)_2}]^{2+}$ (blue) and $[\mathbf{Ru(phtpy)(phen\text{-}hpp)}]^{2+}$ (purple) recorded in deaerated acetonitrile solution at ambient temperature (λex. = 650 nm). The spectra on the left is zoomed to put in evidence the intensity of **1** and **2** compared to the Os^{2+} reference.

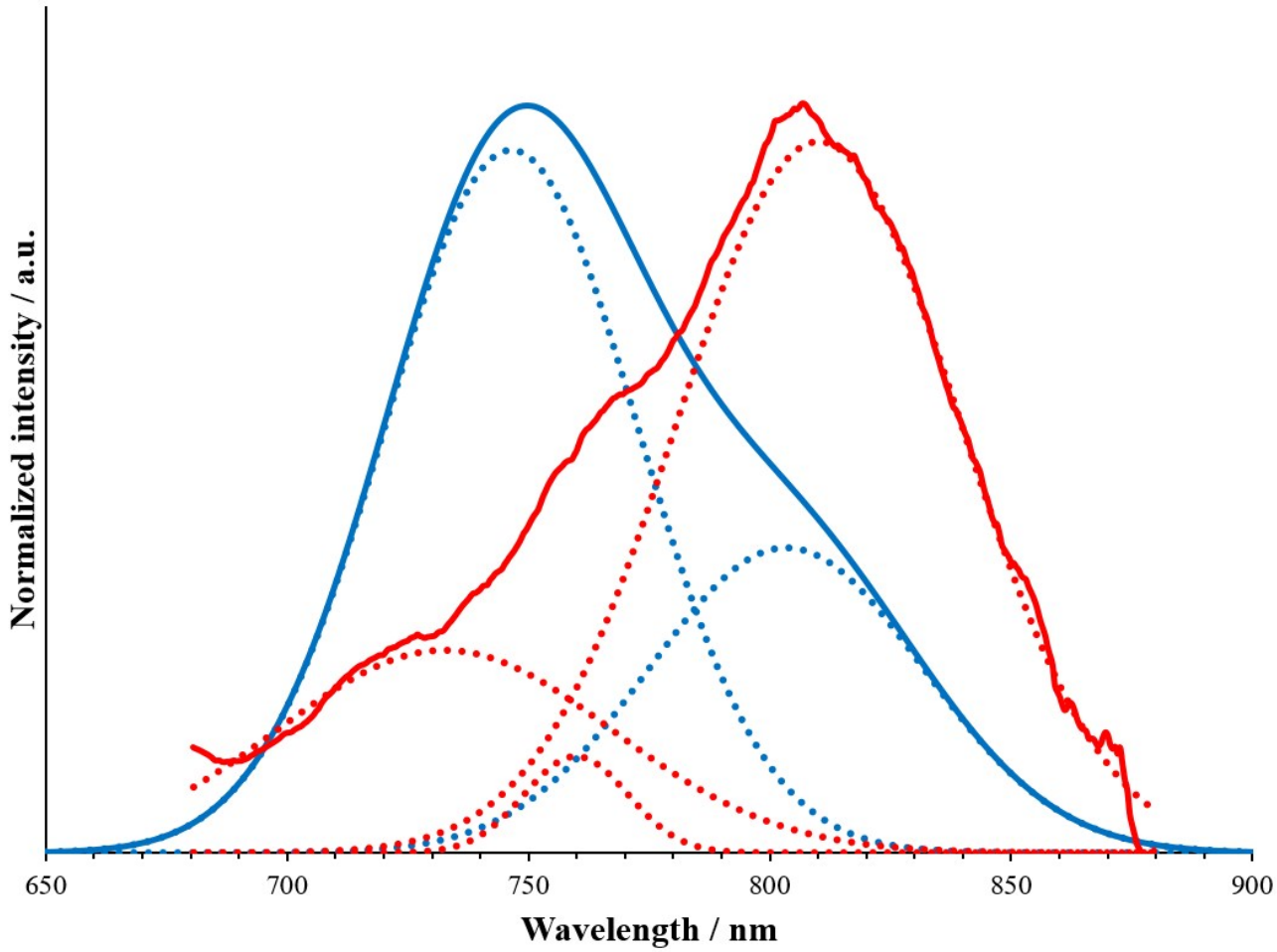

Figure S23. Normalized luminescence spectra of $\mathbf{1}^{2+}$ (red) and $[\mathbf{Os(ttpy)_2}]^{2+}$ (blue) recorded in deaerated acetonitrile solution at ambient temperature along with their respective deconvoluted spectra showing the contributions to the emission (dots curves). The deconvolution fit (95% probability) is > 0.99.

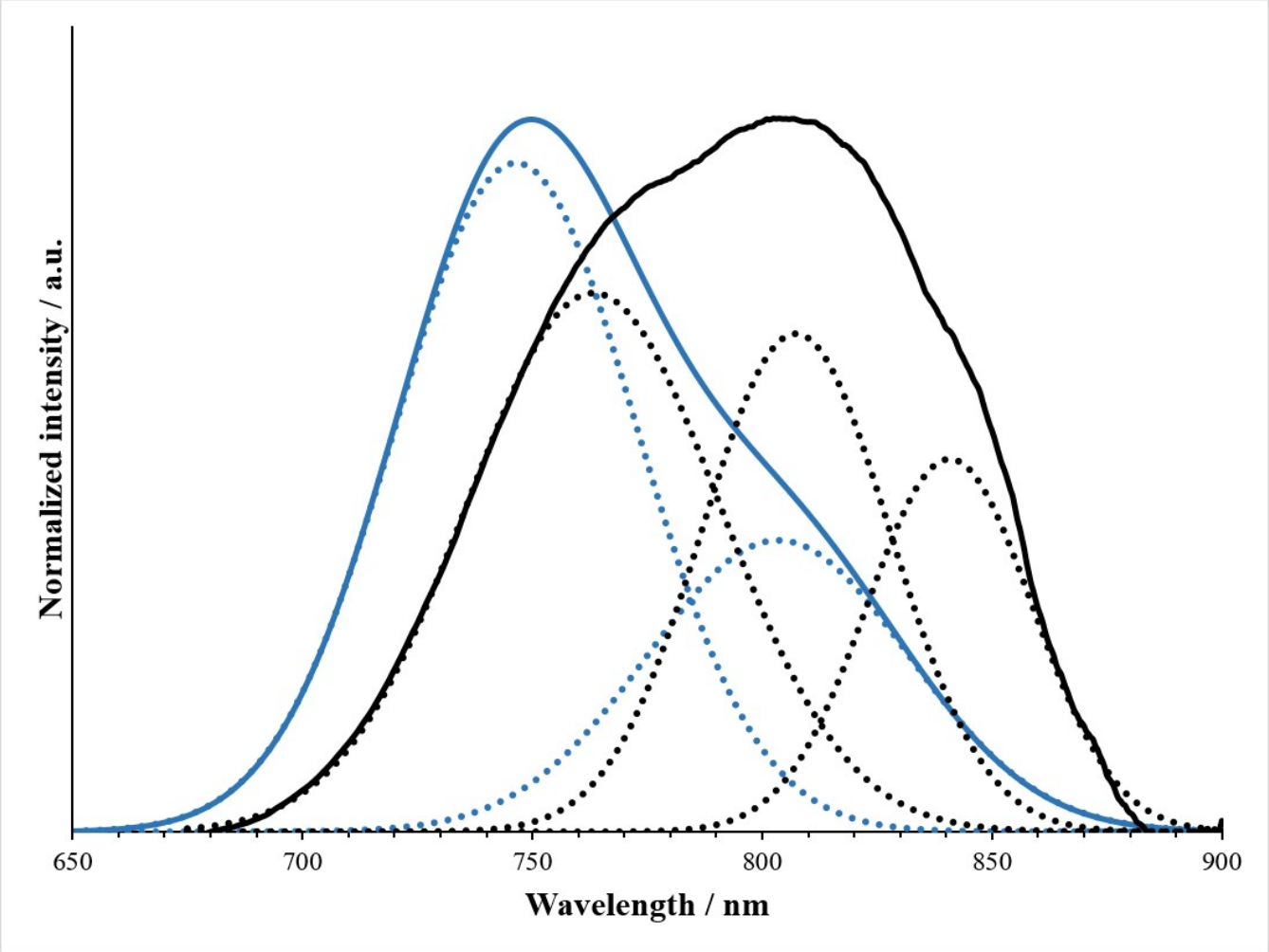

Figure S24. Normalized luminescence spectra of $\mathbf{2}^{6+}$ (black) and $[\mathbf{Os(ttpy)_2}]^{2+}$ (blue) recorded in deaerated acetonitrile solution at ambient temperature along with their respective deconvoluted spectra showing the contributions to the emission (dots curves). The deconvolution fit (95% probability) is > 0.99.

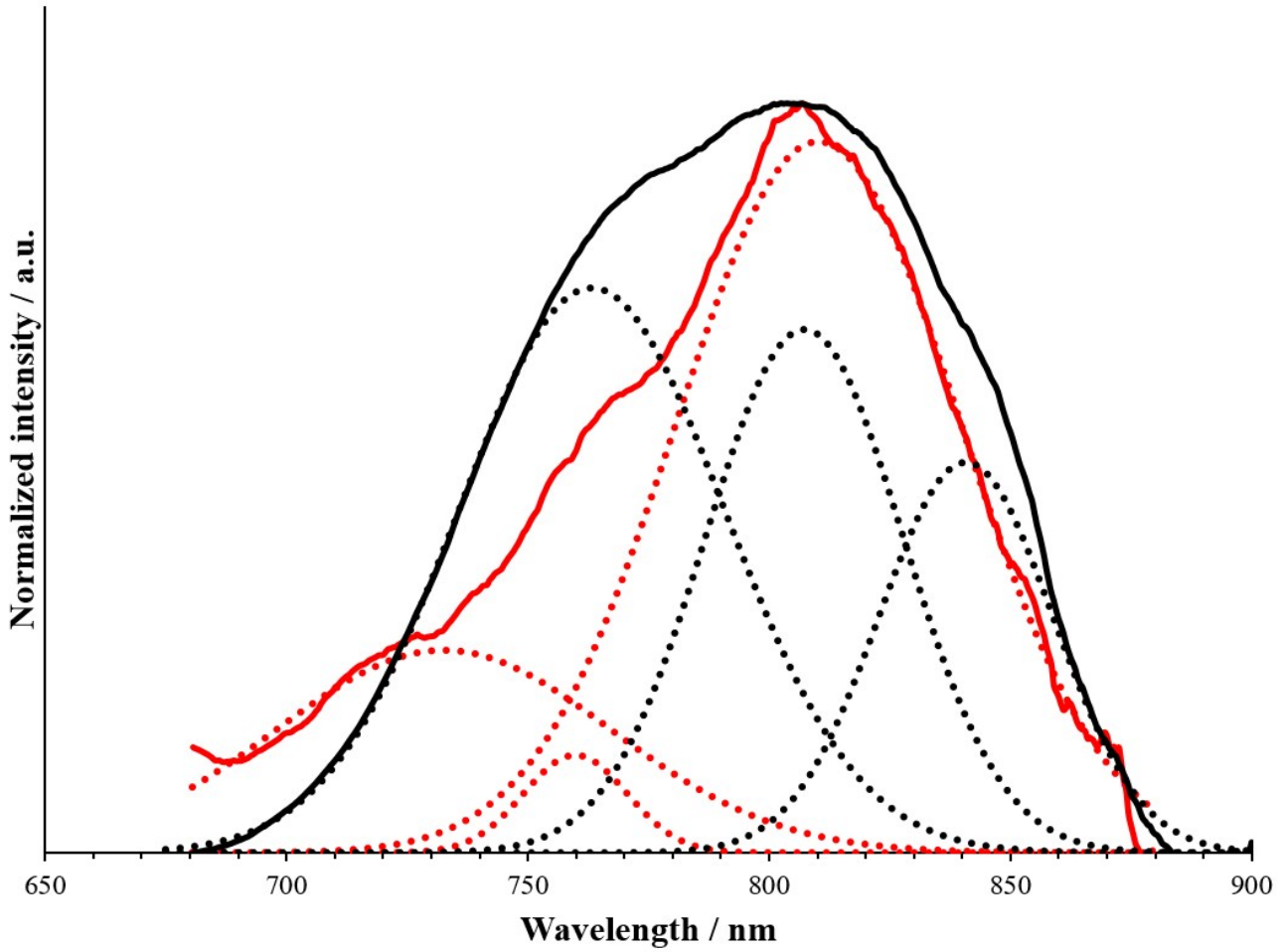

Figure S25. Normalized luminescence spectra of $\mathbf{1}^{2+}$ (red) and $\mathbf{2}^{6+}$ (black) recorded in deaerated acetonitrile solution at ambient temperature along with their respective deconvoluted spectra showing the contributions to the emission (dots curves). The deconvolution fit (95% probability) is > 0.99.

References

[1] M. J. Frisch, G. W. Trucks, H. B. Schlegel, G. E. Scuseria, M. A. Robb, J. R. Cheeseman, G. Scalmani, V. Barone, B. Mennucci, G. A. Petersson, H. Nakatsuji, M. Caricato, X. Li, H. P. Hratchian, A. F. Izmaylov, J. Bloino, G. Zheng, J. L. Sonnenberg, M. Hada, M. Ehara, K. Toyota, R. Fukuda, J. Hasegawa, M. Ishida, T. Nakajima, Y. Honda, O. Kitao, H. Nakai, T. Vreven, J. A. Montgomery Jr., J. E. Peralta, F. Ogliaro, M. J. Bearpark, J. Heyd, E. N. Brothers, K. N. Kudin, V. N. Staroverov, R. Kobayashi, J. Normand, K. Raghavachari, A. P. Rendell, J. C. Burant, S. S. Iyengar, J. Tomasi, M. Cossi, N. Rega, N. J. Millam, M. Klene, J. E. Knox, J. B. Cross, V. Bakken, C. Adamo, J. Jaramillo, R. Gomperts, R. E. Stratmann, O. Yazyev, A. J. Austin, R. Cammi, C. Pomelli, J. W. Ochterski, R. L. Martin, K. Morokuma, V. G. Zakrzewski, G. A. Voth, P. Salvador, J. J. Dannenberg, S. Dapprich, A. D. Daniels, Ö. Farkas, J. B. Foresman, J. V. Ortiz, J. Cioslowski, D. J. Fox, Gaussian, Inc., Wallingford, CT, USA, **2009**.

[2] C. Adamo, V. Barone, *The Journal of Chemical Physics* **1999**, *110*, 6158-6170.

[3] a) J. P. Perdew, K. Burke, M. Ernzerhof, *Physical Review Letters* **1996**, *77*, 3865-3868; b) J. P. Perdew, K. Burke, M. Ernzerhof, *Physical Review Letters* **1997**, *78*, 1396-1396.

[4] a) T. H. Dunning, Jr., P. J. Hay, *Modern Theoretical Chemistry, Vol. 3*, Springer US, New York, **1977**; b) T. H. Dunning, Jr., P. J. Hay, *Methods of Electronic Structure Theory, Vol. 2*, Plenum Press, New York, **1977**; c) J. P. Hay, W. R. Wadt, *The Journal of Chemical Physics* **1985**, *82*, 270; d) W. R. Wadt, J. P. Hay, *The Journal of Chemical Physics* **1985**, *82*, 284; e) J. P. Hay, W. R. Wadt, *The Journal of Chemical Physics* **1985**, *82*, 299.

[5] R. Dennington, T. Keith, J. Millam, 5 ed., Semichem Inc., Shawnee Mission, KS, **2009**.

[6] N. M. O'Boyle, A. L. Tenderholt, K. M. Langner, *J. Comput. Chem.* **2008**, *29*, 839-845.

[7] L. Skripnikov, **2005-2014**.

[8] a) G. S. Hanan, J. Wang, *Synlett* **2005**, 1251-1254; b) B. Laramee-Milette, G. S. Hanan, *Dalton Trans.* **2016**, *45*, 12507-12517; c) A. G. Turner, A. F. Clifford, C. N. Ramachandra Rao, *Anal. Chem.* **1958**, *30*, 1708-1709.

Author Contributions

G.S.H. and B.L.M. conceived and designed the experiments. B.L.M. synthesized the molecular species and performed the characterization as well as the theoretical calculations. G.S.H. and B.L.M. contributed to the writing of the paper.